AD_____

Award Number: W81XWH-11-1-0752

TITLE: Mechanism and therapy for the shared susceptibility to migraine and epilepsy after traumatic brain injury.

PRINCIPAL INVESTIGATOR: K.C. Brennan M.D.

CONTRACTING ORGANIZATION: University of Utah
Salt Lake City UT 84108

REPORT DATE: October 2012

TYPE OF REPORT: Annual

PREPARED FOR: U.S. Army Medical Research and Materiel Command
Fort Detrick, Maryland 21702-5012

REPORT DOCUMENTATION PAGE

Form Approved
OMB No. 0704-0188

1. REPORT DATE	2. REPORT TYPE	3. DATES COVERED
30 October 2012	Annual	30 September 2011 – 29 October 2012

4. TITLE AND SUBTITLE
Mechanism and therapy for the shared susceptibility to migraine and epilepsy after traumatic brain injury.

5a. CONTRACT NUMBER

5b. GRANT NUMBER
W81XWH-11-1-0752

5c. PROGRAM ELEMENT NUMBER

6. AUTHOR(S)
KC Brennan, Ed Dudek, Wendy Pouliot, Jay Vargas, Jorge Manuel Mendez, Punam Sawant.

E-Mail: k.c.brennan@hsc.utah.edu

5d. PROJECT NUMBER

5e. TASK NUMBER

5f. WORK UNIT NUMBER

7. PERFORMING ORGANIZATION NAME(S) AND ADDRESS(ES)
University of Utah
Salt Lake City UT 84108

8. PERFORMING ORGANIZATION REPORT NUMBER

9. SPONSORING / MONITORING AGENCY NAME(S) AND ADDRESS(ES)
U.S. Army Medical Research and Materiel Command
Fort Detrick, Maryland 21702-5012

10. SPONSOR/MONITOR'S ACRONYM(S)

11. SPONSOR/MONITOR'S REPORT NUMBER(S)

12. DISTRIBUTION / AVAILABILITY STATEMENT
Approved for Public Release; Distribution Unlimited

13. SUPPLEMENTARY NOTES

14. ABSTRACT

.
Our proposal studies the natural history and mechanisms of increased brain excitability leading to migraine and epilepsy after traumatic brain injury. In the 6 months since this grant was funded, we have performed experiments spanning nearly the whole range of our proposed work. The most important milestones have been the validation and beginning of data collection for remote telemetric monitoring and two-photon microscopy. These are both technology-intensive, cutting edge techniques, and two-photon microscopy was a new technique for our group. We have also collected publication-ready work using our more familiar optical imaging techniques, showing that the immunological activation associated with TBI alters brain excitability.

15. SUBJECT TERMS- Traumatic brain injury, cortical spreading depression, seizure, post-traumatic headache, post-traumatic epilepsy, migraine, epilepsy.

16. SECURITY CLASSIFICATION OF:			17. LIMITATION OF ABSTRACT	18. NUMBER OF PAGES	19a. NAME OF RESPONSIBLE PERSON
					USAMRMC
a. REPORT	b. ABSTRACT	c. THIS PAGE			19b. TELEPHONE NUMBER *(include area code)*
U	U	U	UU	60	

TABLE OF CONTENTS

INTRODUCTION

Despite great improvements in medical care, traumatic brain injury (TBI) remains the leading cause of death in those under 40 years of age[1,2], in both civilian and military populations. Moreover, as protective strategies and acute treatment have improved, TBI survivors are often profoundly affected by the long-term consequences of injury. These long-term consequences include two disorders of altered brain excitability: chronic headache (usually chronic migraine) and epilepsy. Our proposal examines the links between TBI and these two conditions, which themselves are closely related[3] and can occur in the same patient after injury. Our underlying hypothesis is that the shared susceptibility to migraine and epilepsy after TBI is due to a long-term increase in cortical excitability induced by brain trauma. Specifically:

-We suspect that the secondary injury phase after TBI, characterized by edema, excitation, and profound structural changes, entrains a 'negative' plasticity, which results in long-term aberrant excitation. We will test this with prospective monitoring and mechanism-driven experimental manipulation.

-It is our hypothesis that the glial scar serves as a nidus of hyperexcitability even after conventional recovery is complete. We will test with video EEG monitoring for increased excitability, and will use behavioral measures to test the pain response. We will specifically probe the glial scar and surrounding tissue for evidence of aberrant excitation.

-If development of migraine and epilepsy after TBI is driven by cortical plasticity, modulation of these processes is important, but clinical tolerability is crucial. Memantine is both well tolerated and mechanistically promising; we will test it after CCI as a potential preventive of post-traumatic migraine and epilepsy.

BODY

Task 1. Acute/subacute experiments after controlled cortical impact (CCI) TBI (Brennan, Dudek, Months 1-36)

Task 1.a. Perform CCI, implant monitoring device, and monitor for acute/subacute effects of TBI (7 days after injury)(Dudek, Months 1-9, 24 animals).

Dudek Lab CCI Procedure.

Male, Sprague Dawley rats (n=16) and C57B1/6 mice (n=9) were anesthetized with 2-4% isofluorane and pretreated with atropine (2 mg/kg), and penicillin (0.2 mL, SC, 300,000 IU). The surgical site was shaved, prepped with betadine scrub and solution and isolated with sterile surgical towels. For the CCI procedure, once the rat/mouse was secured in the stereotaxic unit, a rectal probe was inserted and a rectal temperature of 37 ± 0.5 °C was maintained with a temperature-controlled heating pad. Next, a mid-sagittal skin incision was made from the occipital notch to the forehead. A dental drill was used to perform a 6-mm (for rats) or 2-mm (for mice) craniotomy, using bregma, and coronal, lambdoidal, and interparietal sutures as landmarks. A microprobe (Physiotemp) was inserted through a burr hole into the left frontal

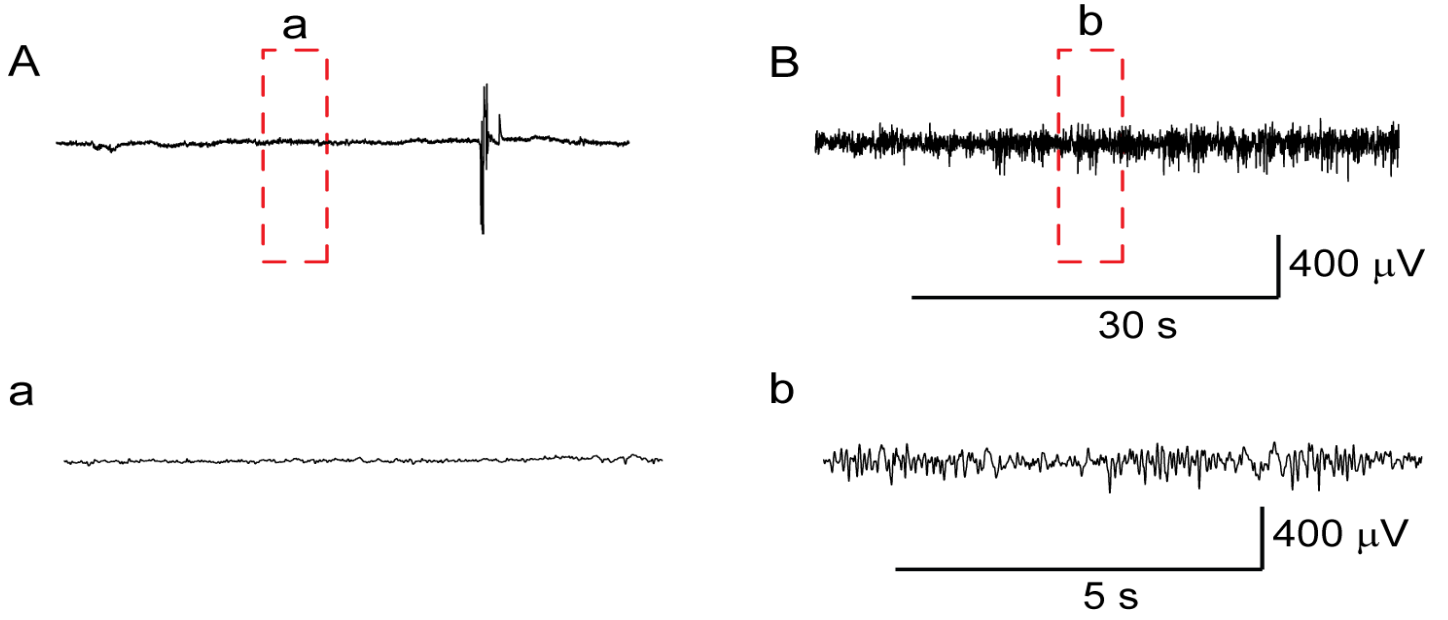

Figure 1: *Baseline EEG recorded from a CCI-treated rat (A) 90 min and (B) 6 hours post CCI injury. (a) and (b) are expanded portions of the EEG traces in the red dashed boxes. Note the suppression of the background activity in the EEG recorded shortly after the injury.*

cortex to monitor brain temperature, which was maintained at 37 ± 0.5 °C by adjusting the warming blanket and warming lights. For the rats, a 5-mm metal impactor tip was pneumatically driven at a velocity of 4.0 m/s, depth of pentration 2.0 mm and duration of 100 msec to induce the traumatic brain injury. For the mice, a 1-mm metal impactor tip was pneumatically driven at a velocity of 4.0 m/s, depth of pentration 1.0 mm and duration of 100 msec to induce the traumatic brain injury. For the rats, six holes were drilled into the skull. Three support screws were screwed into the skull and the three wire EEG electrodes placed on the dura of the contralateral side from the CCI-injury. For the mice, 2 holes were drilled into the skull for the support screws and the two wire EEG electrodes placed on the dura over the CCI-injury site. The entire electrode unit was secured to the skull with dental cement. The skin surrounding the electrode base was sutured shut with non-dissolvable suture. Bupivicane (7.5mg/ml, SC) was applied to all surgical sites. Age-matched sham craniotomies served as controls. Shams underwent anesthesia and preparative surgery but no CCI.

Seizures and possible cortical spreading depression (CSD) after CCI TBI.
To test the hypothesis that acute seizures following a traumatic brain injury may be a predisposing factor for the development of PTE, we subjected mice (n=4) to a moderately severe controlled-cortical impact. Immediately after the impact, the mice were implanted with a novel wireless EEG telemetry device. To serve as a control, sham-operated mice (n=5) underwent the same surgical procedures but were not injured. Video-EEG data were collected for 4 days. Over the

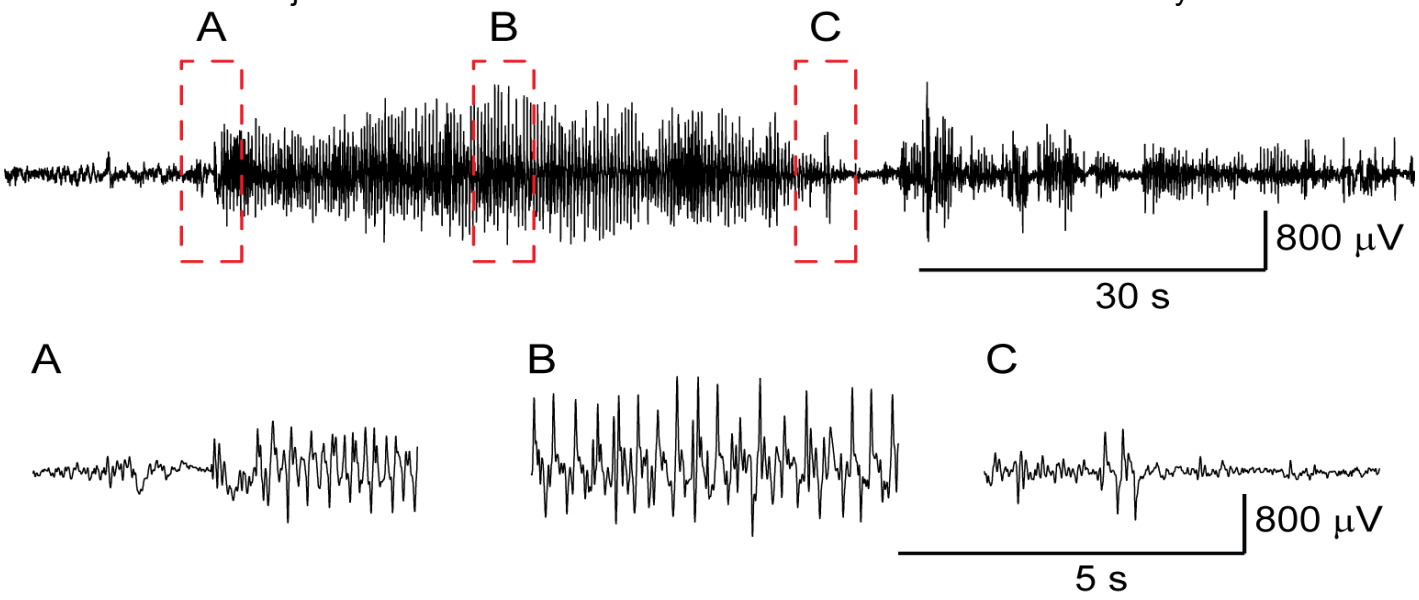

Figure 2: *An example of an electrographic seizure recorded from a CCI-treated rat recorded 3 days post CCI injury. The traces below are expansions of the EEG located in the red dashed boxes. Temporal progression of the beginning (A) middle (B) and end of the seizure (C).*

course of the 4 days, all of the CCI-injured mice died while two of the sham-operated mice had to be euthanized. Unfortunately, due to technical difficulties with the EEG recording bases, the EEG data was compromised. To rectify the problem, we have ordered new EEG recording bases. However, to demonstrate feasibility, we are presenting data from a separately funded project involving rats. In this study, experimental animals (n=5) underwent similar CCI procedures while control animals (n=5) underwent a craniotomy and EEG electrode implantation only. Video-EEG data was recorded within 30 min of the injury and for 3-7 days post CCI-injury with a tether-based EEG recording setup. In the majority of the CCI-injured rats, the background EEG signal was suppressed for several hours (see **Figure 1**). This suppression in background EEG may be caused by spreading depression. Injury-induced seizures were observed in 40% of rats (see **Figure 2**). All of the acute seizures were non-convulsive. There was no mortality in either the CCI-injured or sham-operated groups. Based on the data collected with rats, we believe that it is feasible to record acute seizure activity following a severe traumatic brain injury.

Task 1.b. Perform CCI, thresholding for seizure, cortical spreading depression (Brennan, Months 1-24, 64 animals).

Brennan Lab CCI Procedure.
The Leica Impact One steroteaxic impactor [4] was purchased and tested for its reproducibility of impact parameters (**Figures 3, 4**). The settings used for all experiments thus far have been the following: 4 m/s velocity, 100 ms dwell time, 1 mm impact depth. We have been using a 1 mm diameter flat tipped impactor. So far the device has worked flawlessly. 2 mm craniotomy surgeries have been very successful so far (see Figure 2). All together, 10 animals (GFAP-STAT3-CKO – see below - and WT littermates) have been subjected to the above CCI parameters with a total of 4 animals receiving sham surgery. To test the ability of the new device to deliver a reproducible impact,

3 male animals (2 CKO, 1 WT) were used for testing purposes initially. These animals were sacrificed and brains were harvested to address gross morphological tissue changes 1 week following the impact (see **Task 1.e.** below). A total of 5 male animals (3 CKO, 2 WT) have been utilized thus far that have received the impact and 7 days later CSD susceptibility measured. So far 2 male animals (2 CKO) have been given a sham surgery, where the craniotomy was performed but with no impact. The analysis of CSD susceptibility in the sham-operated group is still in progress. Finally 2 female CKO and 2 female WT animals have been utilized where one CKO animal received CCI the other sham surgery, and one WT received CCI and the other sham surgery. These animals are currently being utilized for preliminary measurement of electrophysiology parameters and cellular alterations using 2-photon microscopy following CCI (see below).

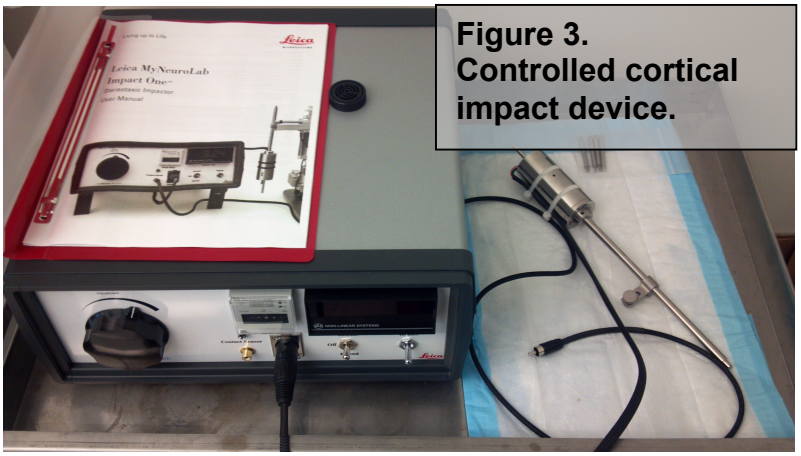

Figure 3. Controlled cortical impact device.

STAT3 conditional knockout (STAT3-CKO) enhance our mechanistic understanding of TBI effects. Our collaborator Dr. Michael Sofroniew was originally going to provide us with mGFAP-YFP mice, which express yellow fluorescent protein in astrocytes, allowing for specific imaging. These mice have unfortunately been inconsistent in their gene expression. As an alternative Dr. Sofroniew has provided us with STAT3-CKO mice. These animals also allow for identification of astrocytes, but also have the significant benefit that they allow testing of a signal pathway involved in astrocyte reactivity after TBI. STAT3-CKO mice, have selective inactivation of STAT3 in astrocytes through the mGFAP promoter and show disrupted glial scarring and attenuated astrogliosis surrounding spinal cord injury [5]. STAT3 is ubiquitous member of the Jak-STAT signaling family, responsible for the signaling of many cytokines and growth factors [6]. STAT3 is expressed by most cell types in the CNS, and is up-regulated following traumatic brain injury in rodents [7]. The time course of phosphorlyated-STAT3 (activated STAT3) was shown to begin shortly after TBI gaining peak levels around 24 hours, and levels returning to baseline at 7-days, with phosphorylated-STAT3 shown to colocalize predominantly with astrocytes [7]. We are beginning to determine the consequences of selectively ablating STAT3 signaling in astrocytes in relation to TBI and cortical excitability, while simultaneously observing the response in the normal astrocytes of wild-type littermates. This tool significantly amplifies the mechanistic power of our proposal. It does increase the number of animals we will use for testing however. The cost of additional animals or experiments (specifically those involving STAT3 transgenic animals; wild-type animal experiments are as we proposed initially) has not and will not be borne by CDMRP unless specifically approved by the program. We will discuss with our Program Officer.

Figure 4. Typical CCI preparation.

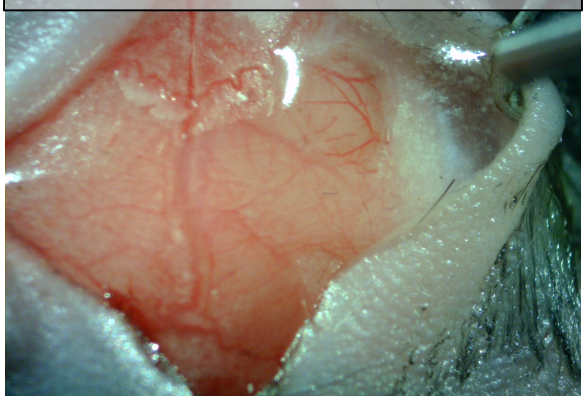

A group of 5 male animals thus far (3 GFAP-STAT3-CKO, and 2 WT littermates) have been subjected to the CCI surgery and CSD susceptibility was measured 7 days following injury. The CSD susceptibility procedure consists of re-opening the now fully healed suture in the anesthetized animal to expose the top of the skull. Carefully placed burr holes (being very cautious not to disrupt the dura matter) are placed in both the injured (ipsilateral) and uninjured (contralateral) hemispheres. Microcapillary tips are placed inside the burr holes producing a constant flow (~3.2 ul/min) of 0.9% saline to start. The animal's vital signs and temperature are monitored throughout the surgery. A thin layer of silicone oil is applied to the top of

the skull to enhance visibility through the skull. Approximately 15 minutes of images taken with a CCD camera using 535 nm LED illumination light (a wavelength that increases hemoglobin contrast) are acquired before the solution perfusing the burrhole is switched to a 1 M KCl to induce CSD events. **Figure 5** displays the preparation. Difference images highlight the reflectance changes associated with CSD. Regions of interest placed in both hemispheres show the OIS fluctuations from each event, example shown in traces above. The number of CSD events in both injured and uninjured hemispheres is recorded for approximately 1 hr following the first CSD event. **Figure 6** shows the results thus far. No statistical power is present thus far, however, the effect of the injury does seem to reduce the number of CSDs in the injured cortex in WT animals more than in KO animals.

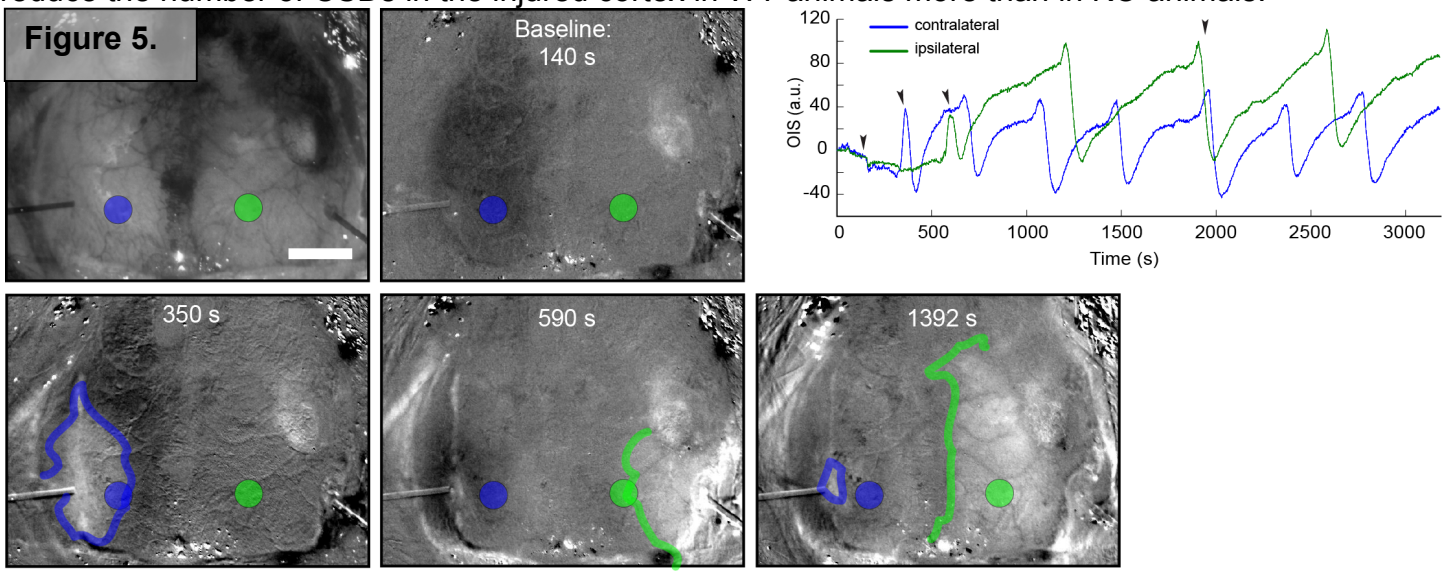

Figure 6.

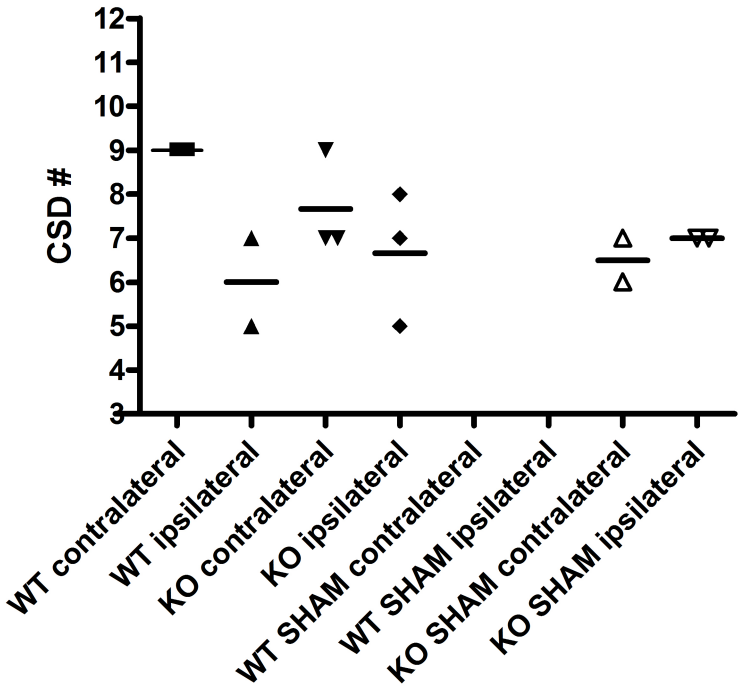

Task 1.c. Perform two-photon experiments 72 hours after CCI (Brennan, Dudek, Months 12-24, 12 animals).

Cell-type specific labeling and subcellular resolution imaging after TBI.
To uncover the cellular processes involved in TBI, we have developed all necessary two photon microscopy methods, in combination with *in vivo* whole-cell electrophysiology techniques (see below). Two-photon microscopy is used to accomplish longitudinal in vivo studies of anatomical changes and to study changes in calcium dynamics, perfusion, and metabolism. The use of transgenic animals with cell type specific fluorescence, like the GAD67-delta neo mouse, expressing green fluorescent protein in interneurons, provides the chance to monitor cell-specific changes caused by the TBI experiment. In addition, the use of astrocytic specific dye (SR101) allows the simultaneous inspection of neuronal and astrocytic changes.

Visualization of astrocytes is important to the goals of the grant, and we have tried different techniques to load SR101. The first techniques consisted in loading the astrocytes by loading SR101 topically in the area of the cortex we wanted to visualize, following the methods described in Nimmerjahn et al 2004 [8]. Briefly, a 100μM solution of SR101 in aCSF was applied to a selected exposed area of the cortex. To have a better loading of the dye, the dura matter should be removed or at least perforated and the solution topically applied for 5 minutes and washed away with aCSF. The second technique consisted of tail vein injection of the dye as described in Appaix et al. 2012 [9]. In this case, 20mg/kg of SR101 in physiological solution is tail vein injected. Usually, after half an hour astrocytes are clearly identified. This technique has proven to be more reliable and with the convenience of not having to further touch the area of the cortex to be imaged (which can artifactually induce astrocyte reactivity).

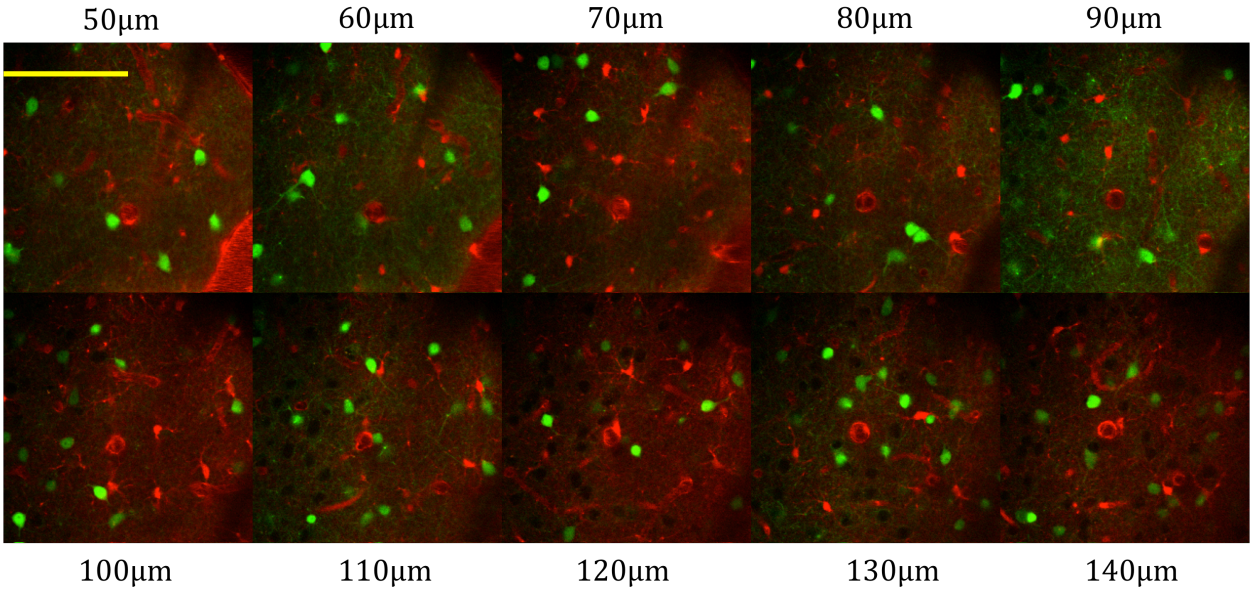

Figure 7: *Two-photon microscope imaging of a GAD67-Δneo mouse with all cortical interneurons identified with GFP and astrocytes stained with SR101. Interneurons are shown in green and astrocytes in red, compatible with fluorophore colors. Though pyramidal neurons are not fluorescent, they are identified by their darker appearance. The scale bar represents 100μm.*

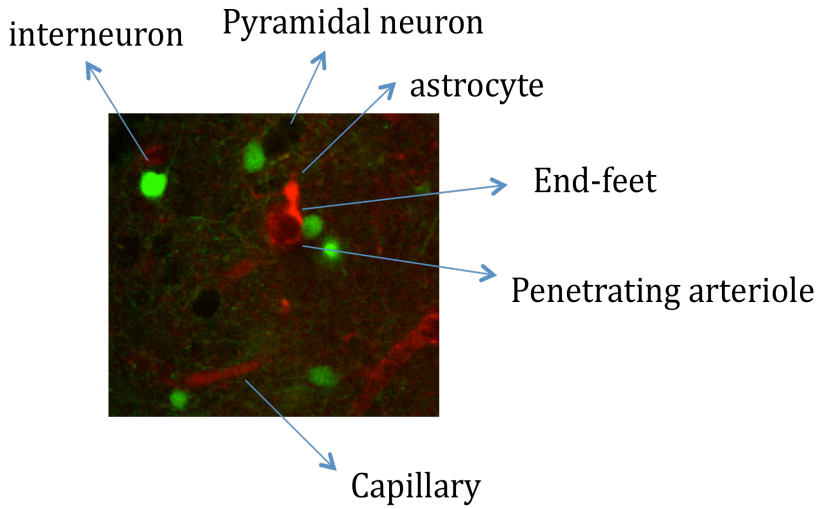

Figure 8: *All the anatomical elements of the network are identified: interneurons, pyramidal neurons, astrocytes and their end-feet, and the vascular components.*

Dendritic beading and cell swelling caused by cortical spreading depression (CSD), which accompanies TBI.

CSD is a massive depolarization that occurs during and after TBI. It causes significant structural and functional changes, including (**Figure 9**) dendritic beading similar to what is seen during ischemia except that it appears to be reversible.

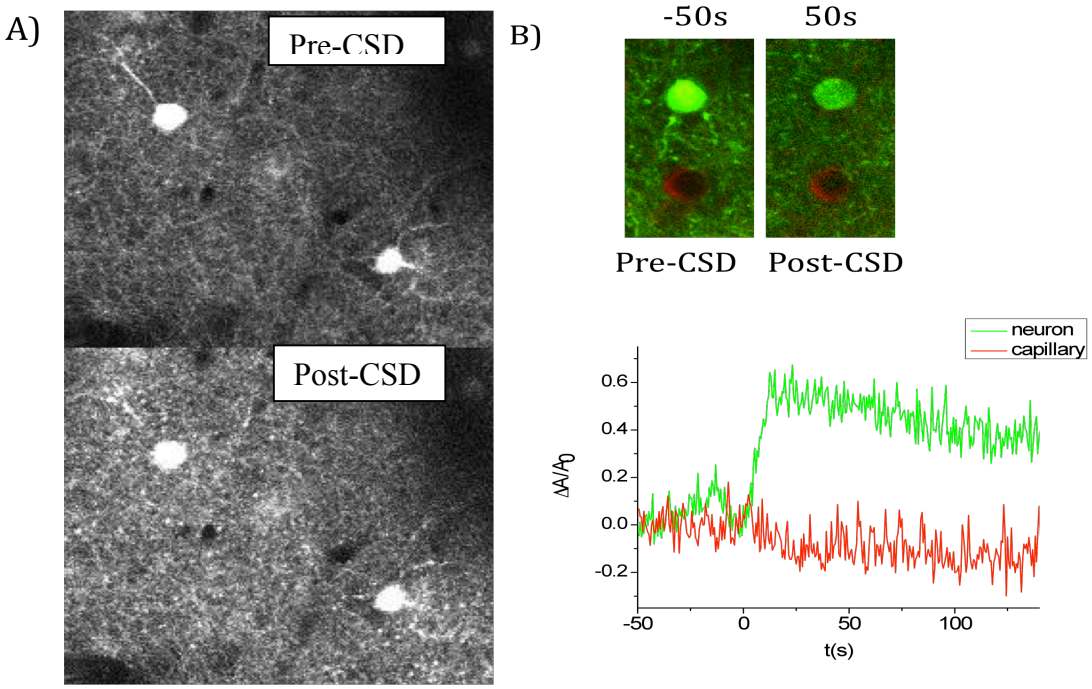

Figure 9: *A) Neuritic beading of the interneurons appears after a CSD event. The beading is visualized as small fluorescent dots in the neural processes. B) Cells swell after CSD. Time traces of the area of the neuron (shown in green) and of a capillary (red) are displayed. The area of the neuron increased more than 50%.*

Alterations in perfusion and metabolism after CSD.

We have implemented methods to monitor blood perfusion and metabolic condition of cortex by two-photon microscopy. By injecting FITC-dextran dyes into the blood a real time quantification of the perfusion is accomplished. Also, the intrinsic fluorescence of the cortex can be monitored providing

information about the NAD/NADH ratio. We have successfully used these techniques to describe changes caused by CSD.

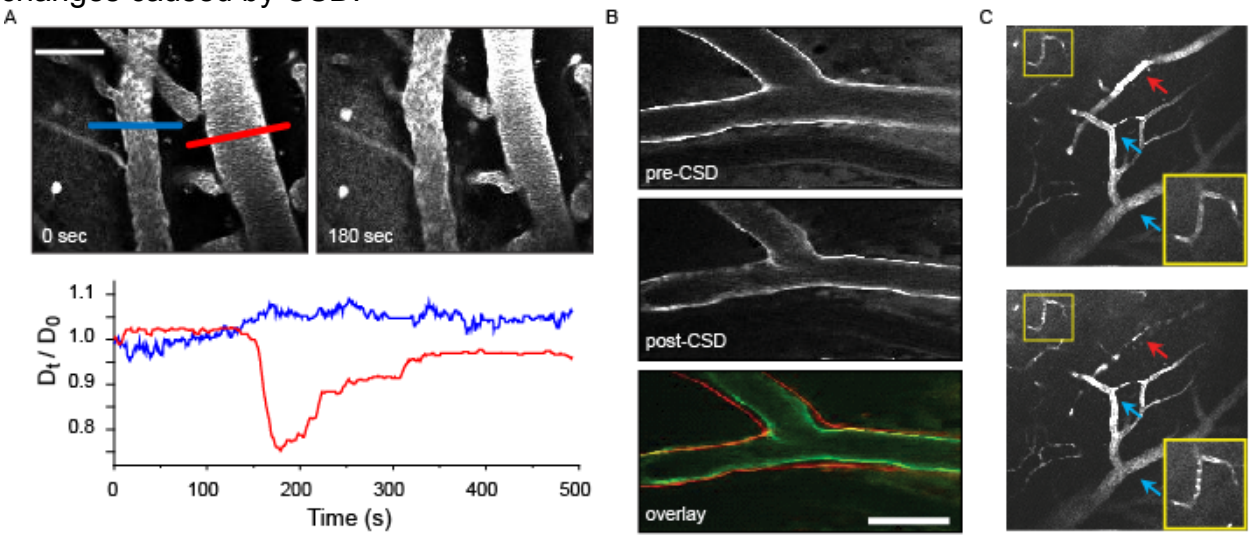

Figure 10: *Massive vascular changes during and after CSD. A. Two photon images of a cortical artery and vein are shown before and during a CSD. Diameter changes were calculated across their cross-section (artery: red, vein: blue) and displayed as time traces in the plot below (scale bar, 50 µm). B. Arteries also undergo morphological changes (labeling of elastin fibers with AlexaFluor 633), becoming more irregular (scale bar, 50 µm). C. Intracortical vascular dynamics during CSD. Images from 50 µm below the cortical surface show penetrating arteriole (red arrow), draining veins (blue arrows) and capillary (yellow inset). Plasma is labeled with 70 kD fluorescein dextran. At baseline, blood flow blurs individual red blood cells (RBCs). During CSD, arteriole (but not vein) constricts massively. Capillary blood flow stops, revealing individual RBCs as dark spots. Shortly after CSD passage, arteriole dilates beyond baseline, but capillary flow is still compromised. Scale: arrows are 50 µm long.*

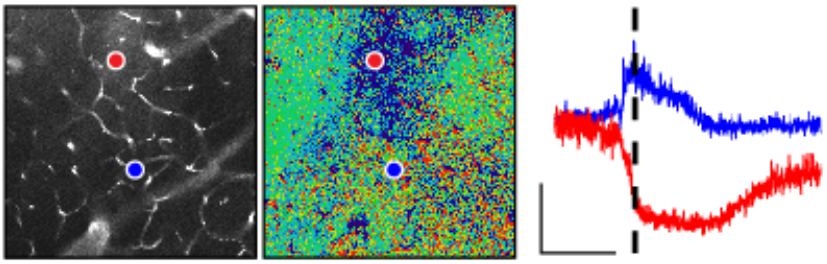

Figure 11: *Fluorescein dextran labeled capillaries 250 µm below the cortical surface (left). NADH intrinsic fluorescence image from same location (center), during peak CSD-associated changes (dashed line on graph). NADH oxidation (red; darkening) and reduction (blue; brightening) can occur, depending on location, however most regions show reduction, consistent with the metabolic challenge of CSD. Calibration: 10% change from baseline; 45 seconds.*

Calcium imaging with Oregon green BAPTA1-AM.

We have implemented calcium imaging of cortical cell populations by bolus loading of Oregon green BAPTA1-AM (OGB). Oregon-Green 488 BAPTA-1 AM is prepared at a concentration of 1 mM. We use a 20% solution of Pluronic F-127 in DMSO and we dissolve 50µg of OGB in it to a concentration of 10 mM. Then this solution is further diluted (to a 1mM solution) in a HEPES aCSF (150mM NaCl, 2.5mM KCl, 10mM Hepes, with a pH of 7.4). The calcium indicator is loaded in a glass pipette and bolus loaded in the cortex at a depth of 200µm (typically using a pressure of 10 PSI for 1 minute) [10]. Imaging is started after an hour of the pressure injections. An example of calcium imaging during CSD event is shown in **Figure 12**. We have now successfully loaded cells with OGB1 AM in the area close to TBI (less than 1mm away from impact, n = 2 animals).

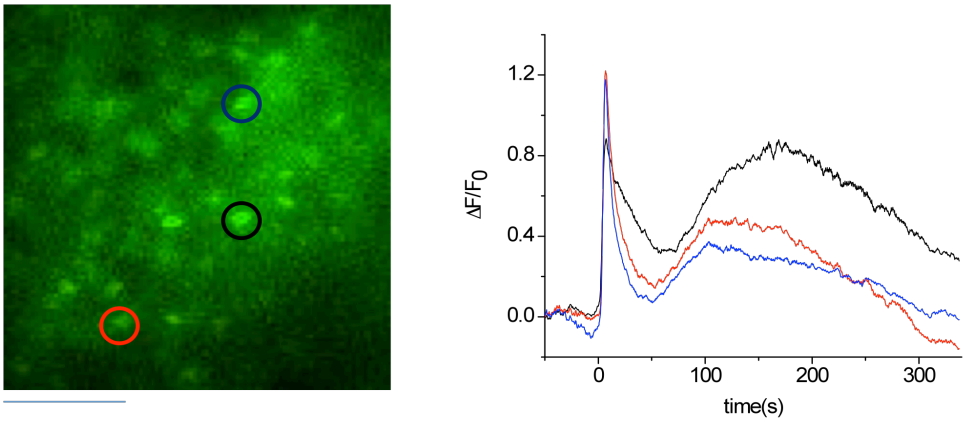

Figure 12. *OGB1 AM loading of a cell population in layer 2/3 of somatosensory cortex (OGB1 selectively labels neurons, but some astrocyte fluorescence is also possible). The fluorescence changes corresponding to the occurrence to a CSD at t=0s in the areas depicted by colored circles are shown in the plot in the right side. The bar indicates 50 μm.*

Imaging with genetically encoded calcium indicators (GECI).

The alternative to dye loading is to use GECI [11,12]. We have explored the used of GCaMP5 delivered by viral vector injections. The use of AAV2/1.hSynap.GCaMP5G(GCaMP3-T302L.R303P.D380Y).WPRE.SV40 reveals neuronal specific population calcium activity in the relevant area of the cortex, because the expression is driven by the neuron-specific Synapsin promoter. For this procedure, the animal is anesthetized with isoflurane (5% for induction and 1.5% for the rest of the procedure) and put in the stereotactic apparatus for the correct identification of the region of interest. A small craniotomy is performed, and a small volume (~1 μL) of the virus suspension is loaded in a glass pipette and pressure injected. The craniotomy is sealed with silicone elastomer and the skin reapposed with vetbond. The animal is administered with antibiotics and analgesics and recovered for 2 or 3 weeks to allow for a sufficient expression of GCaMP. After this the animal is prepared for imaging.

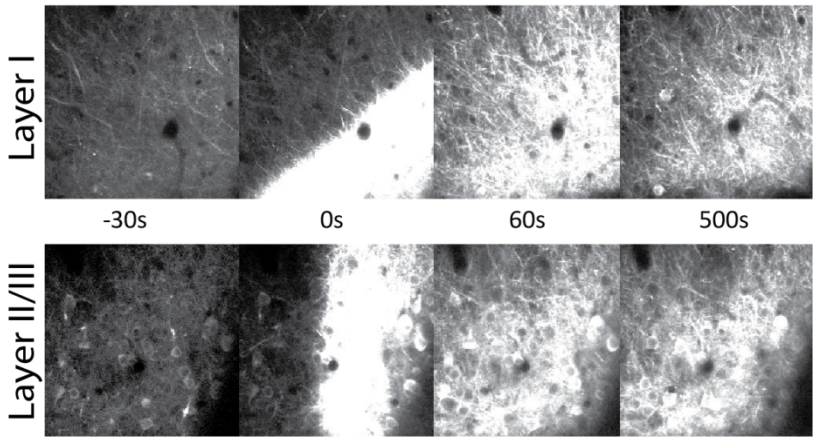

Figure 13: *Layer specific calcium transients in neurons loaded with genetically encoded calcium indicator. An adeno-associated virus encoding GCaMP5 under the synapsin-1 promoter (neuronal specific) was injected in the cortex and 3 weeks later the mouse was prepared for imaging (craniotomy over somatosensory cortex). The same area was imaged at two different depths, corresponding to layer I and layer II/III. Sequences of images show the propagation of the CSD in these two different depths.*

Astrocyte-specific calcium imaging.

We are particularly interested in understanding the astrocytic changes related to TBI. The use of Fluo4-AM yields astrocytic specific calcium signal that can be confirmed with SR-101 labeling [8,10,13].

We have successfully used this dye in WT and in STAT3-CKO animals. The dye loading method was based on the methods described by Hirase et al 2004 [13].

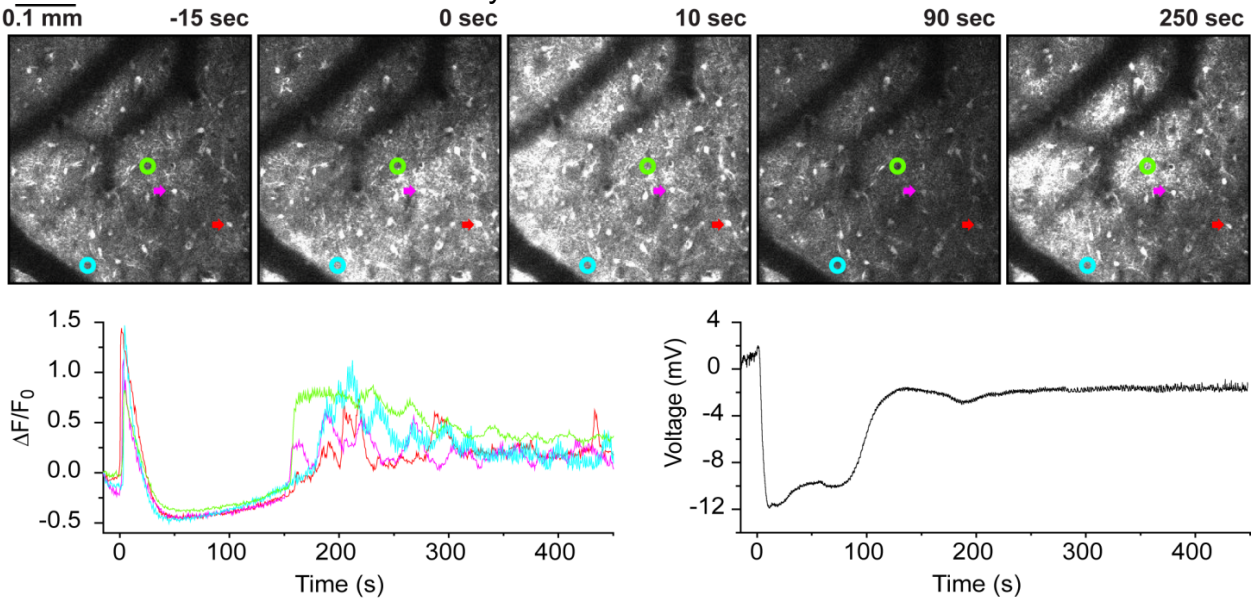

Figure 14: *Massive changes in astrocyte calcium activity during and after CSD. Fluo4-AM was used to load astrocytes in the somatosensory cortex of a WT mouse.* ***A.*** *Time sequence showing the propagation and aftermath of CSD. The wave propagates through the imaging window at 0 s. Colored arrows represent astrocytes and circles represent neuropil. Imaging depth 100 µm.* ***B.*** *Time traces of the fluorescent changes of the astrocytes and neuropil indicated in A. There is a massive increase in astrocyte calcium activity during the wave, followed by a decrease then a subsequent increase to beyond baseline. There is a persistent increase in rhythmic calcium activity. Right hand trace shows field potential deflection associated with CSD, and sustained depolarization after the wave (field potential does not return to baseline) which corresponds temporally with increased calcium activity.*

In vivo *whole cell recording to determine the mechanisms of increased cortical excitability after TBI.*

To study functional changes in cortical neurons after traumatic brain injury, we have used *in vivo* whole cell electrophysiological recordings [14,15]. These recordings will be essential to directly demonstrating synaptic activity associated with sensory processing and behavior.

Surgical Preparation.

Mice (n = 15) were anesthetized using intraperitoneal injection of urethane (1.2- 1.5 g/kg). Body temperature was controlled using a heating pad and maintained at 37°C throughout the experiment. A round craniotomy (approx. 2 mm in diameter) was made in the barrel cortex region (3-4 mm lateral to the midline and 1-2 mm posterior to the bregma). Dura was removed using a 30 gauge syringe needle and fine forceps. Durectomy with less bleeding was an important step in order to have a clean passage for patch electrode through the tissue. Agar (1%) was placed on the brain surface to keep the surface moist.

Electrophysiological Recordings.

Intracellular recordings were performed using thick-wall glass pipettes pulled from borosilicate glass capillaries (OD 1.65 mm, ID 1.2 mm, Garner Glass, Claremont, CA) with a P-87 Flaming-Brown puller (Sutter Instruments, Novato, CA). Patch electrode of 5-7 MΩ was used (tip size of 3-4 µm). A patch pipette was filled with intracellular solution containing (in mM; pH = 7.2): 120 K-gluconate, 1 NaCl, 5 EGTA, 10 HEPES, 1 $MgCl_2$, 130 CsCl, 1 $CaCl_2$, 2 ATP, 0.05 mM Alexa 594 (for visualized experiments). Signals were amplified using an Axoprobe-1D amplifier (Axon Instruments, Foster city, CA) or Multiclamp 700B amplifier. Signals were sampled at 10 kHz and low-passed filtered at 2 kHz. Data were acquired and stored on a PC using a Digidata-1320A digitizer (Clampex, Molecular

Device, Union City, CA), and pClamp 8.2 software (Clampex, Molecular Device, Union City, CA). Electrode was placed on the surface with positive pressure of 30 kPa and advanced to a depth of 100-200 µm. Once the electrode was lowered to the desired cortical depth (layer I-II), pressure was reduced to 4 kPa. In voltage clamp mode, the pipette was moved slowly in steps of 0.04 µm through the layers of the cortex while monitoring the current response to an applied voltage step (10 mV amplitude). We further lowered the pipette until we observed a consistent reduction in response amplitude (approx. 50%), which indicates an increase in electrode resistance. Then positive pressure was removed to zero and suction was applied if necessary to get a gigaseal (a greater than giga-ohm series resistance recorded through the electrode). The command potential of -70 mV was applied. Negative pressure was applied to obtain a whole-cell configuration. Sometimes a gigaseal mode was left without perturbing, to perform cell-attached experiments. In the current-clamp mode, we recorded the spontaneous and evoked activity. Cortical spreading depression was induced by pin-prick and recorded (**Figure 15**).

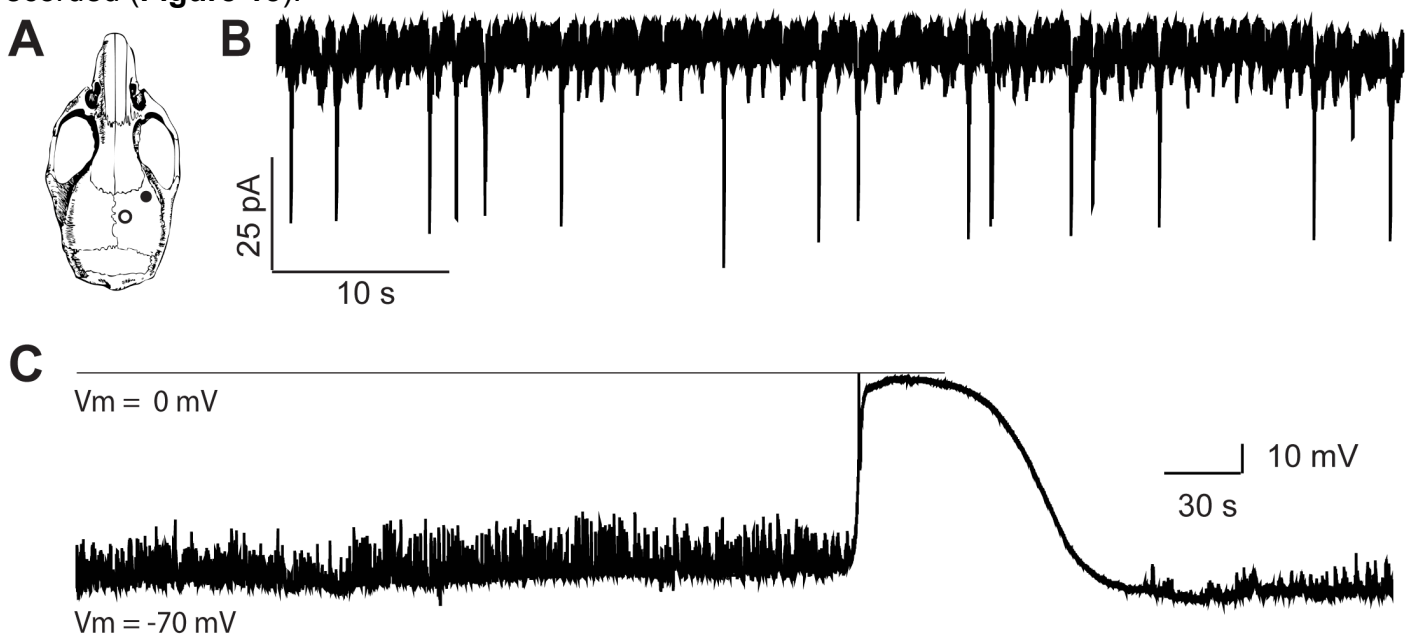

Figure 15: Whole-cell patch clamp recording of CSD in vivo. A. *Schematic representation of the mouse skull demonstrating the location of craniotomy-durectomy for a single-cell recording. Closed and open circles represent locations for electrode placement and CSD induction, respectively.* ***B.*** *Membrane current traces showing spontaneous synaptic activity in layer I-II of somatosensory neurons.* ***C.*** *Membrane potential changes during CSD, measured with patch pipettes filled with K+-gluconate. Following the induction of CSD with pinprick, the membrane potential reached 0mV during the peak of CSD. Note the reduction in neuronal firing after CSD. We will use in vivo whole cell recordings to examine the membrane and synaptic properties of neurons after TBI.*

In another set of experiments, we performed visualized whole-cell recordings using two-photon microscopy. Our approach was to use the 'shadow patching' technique as described in the grant. Briefly, we ejected the fluorescent dye Alexa 594 into the extracellular space. As described by Kitamura et al 2008 [16], individual neurons become visible as dark shadows against the bright fluorescence background. However, in our hands, we were unable to visualize neurons even under high power and different sets of ejection systems. At this stage, we are confident in our skills using blind patch techniques, as well as visualized patch recordings in either GFP or GECI-labelled cells to perform all the experiments outlined in the proposal.

The success rate for whole-cell recordings *in vivo* depends on many factors such as cortical movements, electrode positioning (angle of approach), and the craniotomy preparation. The stability of recordings is mainly associated with breathing and heartbeat-related movements of the animal.

Another issue was to obtain seal resistance between the pipette and cell in a giga-ohm range. We were able to reduce cortical motion by preparing small craniotomies. Anesthetics are known to alter the breathing-associated movements so we tried using different compounds such as urethane or isoflurane or a mixture of both. Pure isoflurane results in poor seal quality, and pure urethane is difficult to control. In our hands, we obtain the fewest artifacts and best anesthetic control with a combination of urethane (0.25 mg/kg, supplemented as necessary) and isoflurane (0.2-0.8 %).

Now that we are obtaining whole-cell recordings in naive animals on a regular basis we have begun testing animals after TBI (n = 2 so far). We will be collecting data from wild-type animals on intrinsic membrane properties, synaptic input during and after sensory, chemical, and electrical stimulation, and cortical spreading depression, in areas near and distant from CCI TBI injury.

Task 1.d. Perform two-photon experiments 72 hours after lipopolysaccharide injection, acutely after hypotonic ACSF perfusion (Brennan, Months 18-30, 36 animals).

Figure 16.

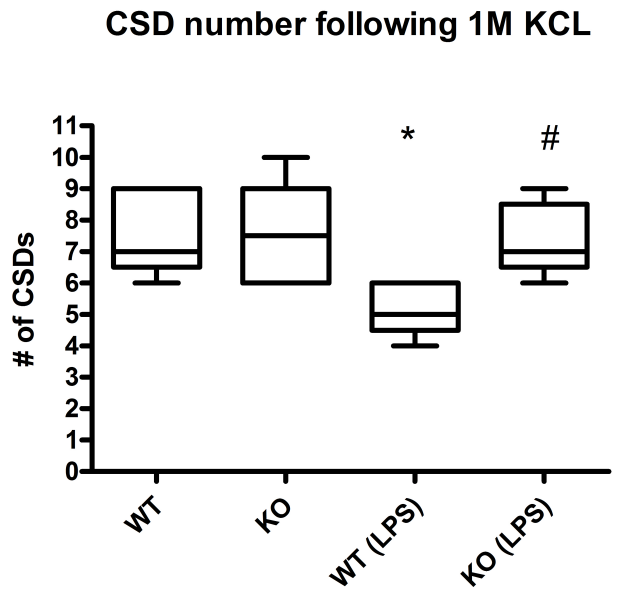

To ascertain the effect of a low dose LPS injection on cortical excitability, a group of 22 male animals was used to determine the effect of LPS exposure to CSD threshold. 6 WT and 6 KO animals were initially used to determine a baseline susceptibly of cortex to 1M KCl induced spreading depression. A subsequent group of 5 WT and 5 KO animals was injected with 0.5 mg/kg LPS i.p. The CSD susceptibility was measured 24 hours later. The CSD number following the first KCl induced event was recorded for 1 hour. The results are shown in Figure 5 (* = WT vs WT(LPS) $P < 0.05$; # = WT(LPS) vs. KO(LPS) $P<0.05$ One-way ANOVA Tukey's Multiple Comparison). LPS treatment reveals a GFAP cell expressing-STAT3 dependent reduction in CSD number in KO animals, an observation not seen in the untreated group. These show that the immunological activation associated with TBI has effects on cortical excitability. It appears that LPS-induced immunological activation reduces cortical excitability, in a manner that is dependent on astrocytic STAT3 signaling pathway function. These results are being supplemented with histology and 2-photon imaging, and will soon be prepared for publication.

Task 1.e. Perform histological analysis on animals 24, 48, 72 hours, and 7 days after CCI TBI (Sofroniew, Brennan, Dudek, Months 1-24, 32 animals).

Preliminary histology using standard methods has been performed so far at the 7 days post injury time point with more histological experiments planned. Methods are being testing in the laboratory now for the routine analysis of TBI tissue – more complex histology will be performed by our collaborator Dr. Michael Sofroniew. **Figure 17** shows the typical lesion pattern following our protocol. **Figure 18** shows Nissl stain at different magnifications. There does appear to be an increased granular staining pattern near the lesion site in KO animal tissue. However, this finding needs to be confirmed with more staining.

Figure 17: *Typical brain after PBS and PFA perfusion, the CCI injury is approximately 2 mm in diameter.*

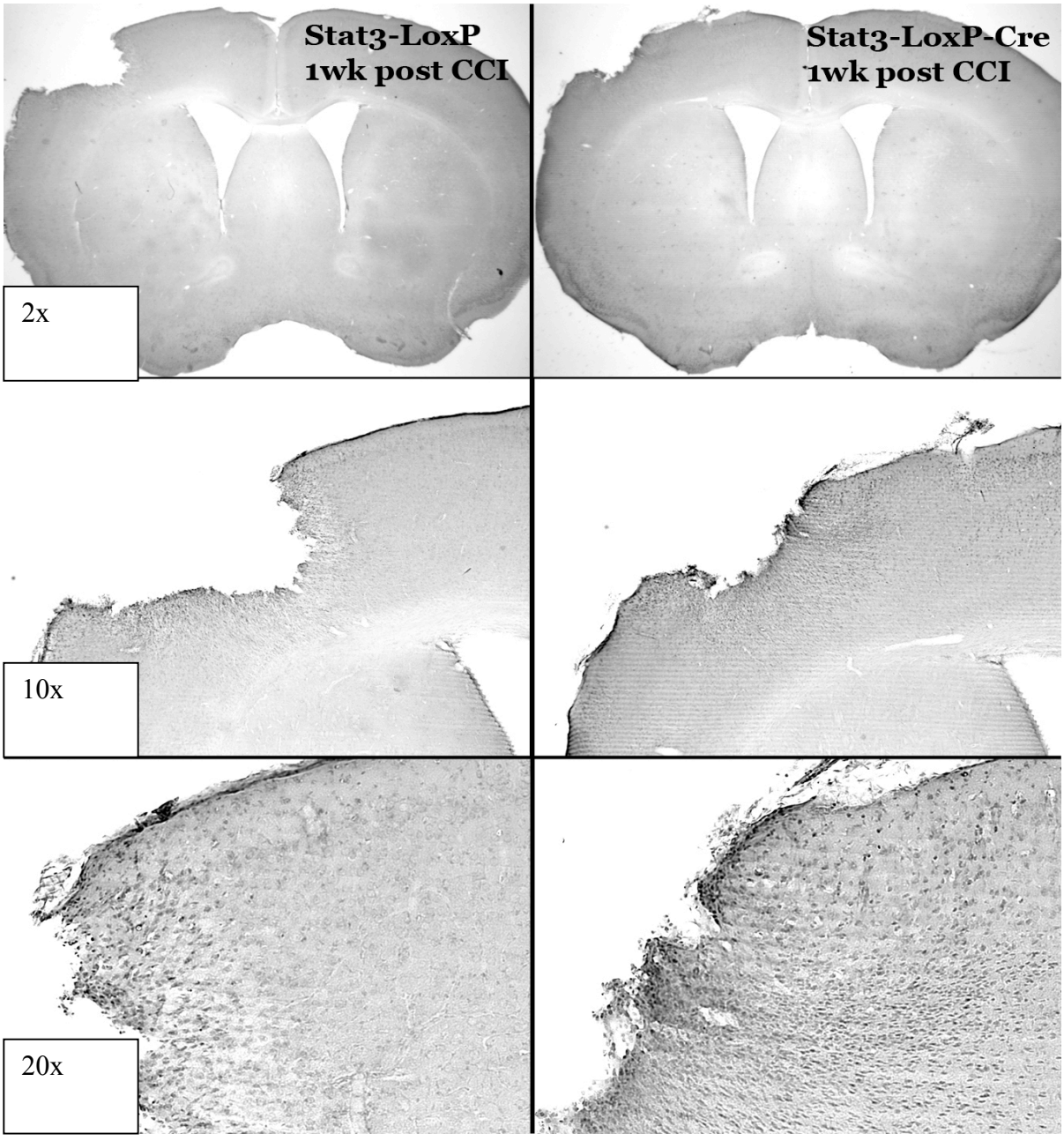

Figure 18. *Light microscopy images of Nissl stain displaying lesion area 1 week following impact in WT (Stat3-LoxP) and KO (Stat3-LoxP-Cre)*

Finally, several new antibodies have been successfully tested in the transgenic mouse lines, and subsequent work will use these antibodies for co-labeling studies. **Figure 19** demonstrates our ability to label neurons (NeuN), microglia (Iba1), and astrocytes (GFAP) in the mouse cortex.

Figure 19.

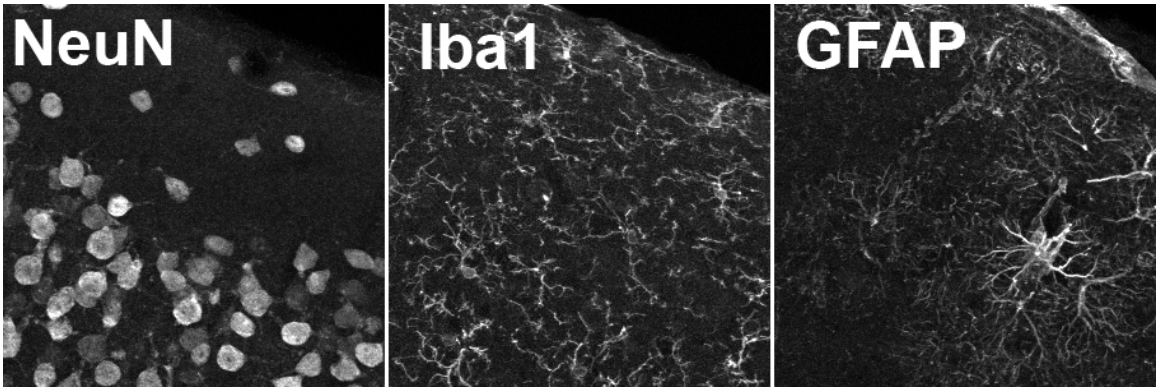

Task 1.f. Perform plasma protein extravasation and brain water content experiments, analysis on animals 24, 48, 72 hours, 7 days after CCI TBI (Brennan/Dudek, Months 1-24, 32 animals).

Pending.

Task 1.g. Analyze results, correlate with histological and other experimental data, prepare data for publication (Brennan/Dudek, Sofroniew, Months 25-36).

Pending.

Task 2. Chronic experiments after CCI TBI (Brennan, Dudek, Months 1-36).

Work in Task 2 pending completion of the bulk of Task 1. Specific sub-tasks are below. However, our preliminary data showing the effects of memantine on recovery from ischemic brain injury (relevant to Tasks 2.b. and 2.h.) have been submitted for publication. The manuscript is attached as **Appendix 1**.

a. **Perform CCI, implant monitoring device, and monitor for chronic effects of TBI (3 months after injury)(Dudek, Months 18-24, 24 animals).**
b. **Perform CCI, implant monitoring device, and monitor for effects of memantine treatment after TBI (3 months after injury)(Dudek, Months 18-24, 32 animals).**
c. **Peform voltage sensitive dye experiments 3 months after CCI (Brennan, Months 24-36, 12 animals).**
d. **Perform CCI, two-photon experiments 3 months after CCI (Brennan, Dudek Months 24-36, 12 animals).**
e. **Perform histological analysis on animals 3 months after CCI TBI (Sofroniew, Brennan, Dudek, Months 18-36, 80 animals).**
f. **Perform plasma protein extravasation and brain water content experiments, analysis on animals 3 months after CCI TBI (Brennan/Dudek, Months 18-36, 40 animals).**
g. **Perform nociception behavior experiments (mechanical and thermal thresholds, rotarod) on animals 3 months after CCI TBI (Bates, Brennan, Months 18-36, 160 animals).**
h. **Perform nociception behavior experiments (mechanical and thermal thresholds, rotarod) on animals 3 months after CCI TBI and treatment with memantine or placebo (Bates, Brennan, Months 18-36, 160 animals).**

i. **Analyze results, correlate with histological and other experimental data, prepare data for publication (Brennan/Dudek, Bates, Sofroniew, months 25-36).**

KEY RESEARCH ACCOMPLISHMENTS

•Optimized controlled cortical impact TBI (CCI) parameters for mouse.

•Implemented two-photon microscopy and whole cell recording *in vivo*, now performing after CCI.

•Performing continuous EEG monitoring of mice after CCI to monitor for seizures and cortical spreading depression (CSD).

•Showed that lipopolysaccharide (LPS) treatment, used to model inflammatory effects of TBI, reduces susceptibility CSD, but not in mice where astrocyte STAT3 signaling disrupted.

•Measuring susceptibility to CSD after CCI.

REPORTABLE OUTCOMES

•None so far. However LPS results are publication-ready, when supplemented by histology and 2-photon imaging.

CONCLUSION

In the first six months since the funding of this award we have established and validated all the experimental techniques we will need for the completion of the project, and have begun collecting data in earnest. We are now collecting publication-ready data for each sub-task and already have publication-ready data showing effects of TBI-associated immune activation on cortical excitability. Our next steps will be to complete acute experiments measuring CSD susceptibility, neuronal excitability, and astrocyte calcium activity after CCI, and begin chronic experiments measuring long-term sequelae of TBI and their modulation with memantine. We are also attempting to extend our present work in order to maximize military-relevant synergies: we have applied for a VA Merit Award extending the present research; in doing so we have begun a collaboration with a University of Utah engineer (Dr. Kenneth Monson) performing blast TBI. Blast TBI is not part of this grant but enhances our ability to model all effects of military TBI. In addition, with co-investigator Dr. Ed Dudek, we have entered collaboration with University of Utah and Wahlen VA imaging researchers (Drs. Deborah Yurgelun-Todd, Melissa Lopez-Larson, and Perry Renshaw) measuring other comorbidities (PTSD, depression) of TBI. We are planning a DOD or VA program grant application incorporating human and animal research.

So what?
If successful our work will:
•Define the natural history of excitable events in the brain after TBI.
•Determine the mechanisms of these excitable events.
•Develop treatments that prevent the progression to migraine and epilepsy after TBI.
If we achieve our goals, they will have a measurable impact on the quality of life of our service personnel, our veterans, and the civilian TBI population.

REFERENCES

1. Bruns, J. & Hauser, W. A. The Epidemiology of Traumatic Brain Injury: A Review. *Epilepsia* **44**, 2–10 (2003).
2. Ghajar, J. Traumatic brain injury. *Lancet* **356**, 923–929 (2000).
3. Rogawski, M. A. Common pathophysiologic mechanisms in migraine and epilepsy. *Arch. Neurol* **65**, 709–714 (2008).
4. Brody, D. L. *et al.* Electromagnetic controlled cortical impact device for precise, graded experimental traumatic brain injury. *J. Neurotrauma* **24**, 657–673 (2007).
5. Herrmann, J. E. *et al.* STAT3 is a critical regulator of astrogliosis and scar formation after spinal cord injury. *J. Neurosci* **28**, 7231–7243 (2008).
6. Aaronson, D. S. & Horvath, C. M. A road map for those who don't know JAK-STAT. *Science* **296**, 1653–1655 (2002).
7. Oliva, A. A., Jr, Kang, Y., Sanchez-Molano, J., Furones, C. & Atkins, C. M. STAT3 signaling after traumatic brain injury. *J. Neurochem.* **120**, 710–720 (2012).
8. Nimmerjahn, A., Kirchhoff, F., Kerr, J. N. D. & Helmchen, F. Sulforhodamine 101 as a specific marker of astroglia in the neocortex in vivo. *Nat Meth* **1**, 31–37 (2004).
9. Appaix, F. *et al.* Specific in vivo staining of astrocytes in the whole brain after intravenous injection of sulforhodamine dyes. *PLoS ONE* **7**, e35169 (2012).
10. Stosiek, C., Garaschuk, O., Holthoff, K. & Konnerth, A. In vivo two-photon calcium imaging of neuronal networks. *PNAS* **100**, 7319–7324 (2003).
11. Tian, L. *et al.* Imaging neural activity in worms, flies and mice with improved GCaMP calcium indicators. *Nat Meth* **6**, 875–881 (2009).
12. Zariwala, H. A. *et al.* A Cre-Dependent GCaMP3 Reporter Mouse for Neuronal Imaging In Vivo. *J. Neurosci.* **32**, 3131–3141 (2012).
13. Hirase, H., Qian, L., Barthó, P. & Buzsáki, G. Calcium Dynamics of Cortical Astrocytic Networks In Vivo. *PLoS Biol* **2**, e96 (2004).
14. Margrie, T., Brecht, M. & Sakmann, B. In vivo, low-resistance, whole-cell recordings from neurons in the anaesthetized and awake mammalian brain. *Pflügers Archiv European Journal of Physiology* **444**, 491–498 (2002).
15. Isaacson, J. S. & Scanziani, M. How inhibition shapes cortical activity. *Neuron* **72**, 231–243 (2011).
16. Kitamura, K., Judkewitz, B., Kano, M., Denk, W. & Häusser, M. Targeted patch-clamp recordings and single-cell electroporation of unlabeled neurons in vivo. *Nat. Methods* **5**, 61–67 (2008).

APPENDICES

Appendix 1: Submitted Manuscript: *Memantine enhances recovery from stroke.*

Memantine enhances recovery from stroke.

Running title: Memantine in stroke recovery.

Héctor E. López-Valdés[1*], Andrew N. Clarkson[1,2*], Yan Ao[3], Andrew C. Charles[1], S. Thomas Carmichael[1], Michael V. Sofroniew[3], and K.C. Brennan[1,4**]

1. Department of Neurology, David Geffen School of Medicine at UCLA

2. Departments of Anatomy and Psychology, University of Otago, NZ.

3. Department of Neurobiology, David Geffen School of Medicine at UCLA

4. Present Address: Department of Neurology, University of Utah School of Medicine

*These authors contributed equally to this work.

**To whom correspondence should be addressed.

383 Colorow Drive, Room 364, Salt Lake City UT 84103.

k.c.brennan@hsc.utah.edu.

HLV and KCB conceived and designed the experiments, HLV, ANC, and YA performed the experiments, HLV, ANC, and KCB analyzed the data, STC, ACC, and MVS assisted in experimental design, analysis, and manuscript drafting, and HLV and KCB wrote the manuscript.

Funding information: This work was supported by the National Institutes of health (NS059072 (KCB); NS070084 (KCB); NS053957 (STC); NS057624 (MVS); an American Heart Association Postdoctoral Fellowship, a Repatriation Fellowship from the New Zealand Neurological Foundation and the Sir Charles Hercus Fellowship from the Health Research Council of New Zealand (ANC); and the Larry L. Hillblom Foundation (HLV, STC, ACC).

The authors have no conflicts of interest to disclose.

Abstract

Stroke treatment is constrained by extremely limited treatment windows, and the clinical inefficacy of agents that showed preclinical promise. Yet animal and clinical data suggest considerable post-stroke plasticity, which could allow for treatment with recovery-modulating agents. Memantine (MEM) is a well-tolerated N-methyl D-aspartate (NMDA) glutamate receptor antagonist in common use for Alzheimer's disease. MEM, 30mg/kg/day, or vehicle, was delivered chronically in drinking water beginning more than 2 hours after photothrombotic stroke. No difference in infarct size or neuronal number was noted, showing that no neuroprotective effects were present. However, mice treated chronically with MEM showed significant improvements in motor control as measured by cylinder test and grid walking performance compared to vehicle treated animals. Optical intrinsic signal (OIS) imaging revealed an increased area of forepaw sensory maps. There was decreased reactive astrogliosis and increased vascular density around the infarcted cortex. Peri-infarct Western blots revealed increased brain-derived neurotrophic factor (BDNF) and phosphorylated-Tropomyosin-related kinase B receptor (p-TrkB) expression. Our results suggest that MEM improves stroke outcome in a non-neuroprotective manner involving increased BDNF signaling, reduced reactive astrogliosis and improved vascularization, associated with improved recovery of sensory and motor cortical function. The clinical availability and tolerability of MEM allow for immediate clinical translation if warranted.

Introduction

Stroke is the second leading cause of death, and is a major cause of morbidity worldwide (Kinlay, 2011; Roger et al., 2012). Despite an enormous amount of preclinical and clinical research, treatment options are limited. The use of tissue plasminogen activator (the only FDA-approved treatment for stroke) is restricted to the few hours after stroke, and beyond this narrow time window treatment is limited to supportive care, secondary prevention, and rehabilitation techniques (Zhang and Chopp, 2009; Benowitz and Carmichael, 2010; Carmichael, 2010).

Neuroprotection, the prevention of cell death beyond the boundaries of the infarct core, has held great preclinical promise for many years. However the significant protective effects seen in animal models have failed to be translated to clinical use, in large part because of the clinical inefficacy of the agents used in animal models.

Despite the loss of neuronal tissue, considerable plasticity is retained after stroke in both animal models and in humans. The manipulation of the recovery process has emerged as an alternative and potentially more tractable target in stroke research (Zhang and Chopp, 2009; Clarkson et al., 2010, 2011).

Memantine (MEM) is a non-competitive, use-dependent NMDA antagonist, which is in common clinical use for treatment of moderate to severe Alzheimer's disease (Rammes et al., 2008; Thomas and Grossberg, 2009). As an NMDA antagonist, MEM has been tested for neuroprotective effects and has been found to reduce infarct size when given acutely (Chen et al. 1998; Görgülü et al. 2000; Lapchak 2006; Hao et al. 2008; Liu et al. 2009; Babu & Ramanathan 2009). However, MEM has other effects that may be relevant beyond the acute setting. For example, MEM treatment causes an increase in secretion of brain-derived neurotrophic factor (BDNF)(Marvanová et al., 2001; Meisner et al., 2008), which is involved in cortical plasticity after stroke (Murphy and Corbett, 2009; Clarkson et al., 2011).

We treated mice chronically with MEM or vehicle more than 2 hours after stroke, in order to minimize MEM's known neuroprotective effects. We used doses specifically designed to mimic serum concentrations in humans (Minkeviciene et al., 2004). We found that despite an absence of neuroprotection, MEM improved stroke outcome as measured by behavioral testing and recovery of functional sensory maps. This effect was associated with decreased reactive astrogliosis, increased vascular density, and increased BDNF and p-TrkB expression. Given the tolerability of MEM in an aged population with characteristics similar to stroke patients, our results may have direct translational relevance.

Methods

Animals

Male C57BL/6J mice (n = 40; 28-32 g) were housed under a 12-hour light/dark cycle with *ad libitum* access to food and water. All protocols were approved by the Animal Research Committee of the University of California.

Induction of Focal Ischemia

Animals were anesthetized with isoflurane (4% induction and 2.0-2.5% maintenance) and placed in a stereotactic frame. A small amount of petrolatum was placed in both eyes to avoid corneal drying. The head was shaved and providone-iodine solution was applied and subsequently cleaned with 70% ethanol. A midline scalp incision exposed the skull overlying the left motor and somatosensory cortex and the skin was retracted. A cold light source (KL1500 LCD, Zeiss) attached to a 40× objective and giving a 2-mm diameter circle of illumination was positioned 1.5 mm lateral from Bregma (centered over forepaw (FP) motor cortex, but affecting hindpaw (HP) motor cortex, FP and HP sensory cortex, and supplementary motor areas as well – see **Figure 1B**). Rose Bengal (200µl of a 10mg/ml solution; Sigma) was injected intraperitoneally 5 minutes prior to induction of photothrombosis, which was induced following fifteen minutes of irradiation.

Optical Intrinsic Signal (OIS) Imaging

Surgery and recovery. Animals were imaged 7 days before and 7, 14 and 28 days after focal ischemia. Mice were anesthetized with enflurane (4% induction and 1.5- 2% maintenance) and placed in a stereotactic frame. Sterile scalp preparation and skull exposure was performed as above. The skull was cleaned with sterile saline solution and the periosteum was removed carefully with small forceps. To increase the translucency of the skull, sterile silicone oil was applied. During imaging, anesthesia was adjusted to maintain a respiratory frequency of 100-120 breaths per minute, a corneal blink reflex and no response to toe pinch. Body temperature was monitored and maintained at 37.0 °C with a homeothermic blanket (Harvard Apparatus). At the end of the experiment, the scalp was cleaned with sterile saline solution and sutured (6-0 silk), and antibiotic (Animax

cream, Pharmaderm) was applied over the suture. Sterile saline solution (0.4 mL) was injected subcutaneously for hydration, and the animals were allowed to recover in a warmed environment.

Image acquisition. A cooled 16-bit CCD camera (Photon Max 512B, Princeton Instruments) connected to a tandem lens system (two 25-mm f/0.95 Cosmicar/Pentax CCTV lenses, attached front to front, 1X magnification, field of view 6.6 mm and pixel size 0.016mm) was used to acquire cortical reflectance signal. The cortical surface vessels of the left hemisphere were recorded through the intact skull, during illumination with either a white or green LED light source (Luxeon III, 5550 K; and 530 nm, FWHM 18 nm respectively; Phillips Lumileds); these vessels, along with the bony landmarks (bregma and lambda) served as an anatomical reference. After that, the field of view was defocused 300-350 μm below the vessels, and the illumination was changed to red LEDs (Luxeon III, 617 nm; FWHM 18 nm), which were used for the rest of the experiment. Illumination was adjusted to be even across the imaged field, at an intensity approximately 60% of the camera's dynamic range. Images were acquired at 2 Hz with a 400 ms exposure time.

Generation of functional maps. Electrical stimulation (50Hz, 0.001 s pulse width, 0.14-0.22 mA) was generated by a pulse stimulator (Master 8, A.M.P.I.), connected to a stimulus isolator (Iso-Flex, A.M.P.I.) and delivered to the tissue through pair of subdermal needle electrodes (27 GA; Rochester Electro-Medical, Inc.) which were inserted 2 mm apart under the proximal and distal walking pads of the right FP and HP. The electrical stimulation was delivered 5 s after the start of each trial, and the total duration of one trial was 25 s. An image session consisted of 32 trials for each FP and HP, with an intertrial interval of 5 s, alternating between FP and HP. Images were acquired with WinView software (Princeton Instruments). Image acquisition and electric stimulation were controlled with a custom LabView (National Instruments) virtual instrument.

Memantine Treatment

Mice were treated for 28 days with memantine (1-amino-3,5-dimethyl-adamantane; Sigma) HCL (30 mg/kg/day in a 2% sucrose solution (Minkeviciene et al., 2004)) or vehicle only (2% sucrose) delivered continuously in

drinking water beginning more than 2hrs after stroke. This dosing regimen results in serum concentrations of ~1μM in C57Bl/6J mice, comparable to the therapeutic plasma concentration in humans (Kornhuber and Quack, 1995; Minkeviciene et al., 2004) Animals were returned to their home cage for recovery from the photothrombosis procedure. Animals had been hydrated prior to recovery (see above) and food pellets moistened with MEM-free water were available on the floor of the cage. MEM in drinking water was delivered 2 hours after placement in the cage. Typically, animals did not begin drinking from the mounted cage bottle until 2-4 hours after placement in the cage.

Data Processing and Analysis.

Sensory evoked changes in cortical light reflectance are typically 0.1 % or less of the total intensity of the reflected light (Grinvald et al., 1986; Frostig et al., 1990), so signaling averaging was performed. Sixteen-bit data collected for each trial were converted to 32 bit, to preserve the data resolution and dynamic range during subsequent analysis, and then normalized trial by trial according to the formula $\Delta R/R$, where $\Delta R = Rx - R$. Rx is the data collected during a given 0.5 s frame, and R is the average of 9 frames collected before the stimulus. For an anatomically homogeneous comparison between sessions and animals, a 2 mm square region of interest (ROI) was centered 1.68 mm lateral and 0.53 mm posterior to bregma for HP, and 2.18 mm lateral and 0.08 mm anterior to bregma for FP, based on atlas coordinates (**Figure 1B**) (Franklin and Paxinos, 1997). In all experiments the FP or HP maps were within the boundaries of the ROI.

Quantification of Active Area. Normalized images were processed with a Gaussian filter (half-width, 3 pixels) to remove high frequency noise and a signal threshold was set at 50 % of the maximal response. Functional response area was quantified from the image where maximum reflectance change was noted (this was either 1.5 or 2.0 s after stimulus onset), and all the pixels beyond signal threshold were summed and converted to mm^2. Image analysis was performed using either plugins or custom routines written for ImageJ 1.40g (Rasband, 1997).

Behavioral testing and analysis

Cylinder test and grid-walking test were performed 7 days before, and 7, 14, 21, and 28 days after stroke (**Figure 1A**). *Cylinder test*. Animals were placed in a clear acrylic cylinder (15 cm height; 10 cm diameter) and were videotaped for 10 min in order to determine forelimb preference. Video footage was analyzed offline by raters blind as to the treatment groups. The total number of cylinder contacts with left, right and both forelimbs were counted and the index for preference was obtained following the formula: Index = (Left – Right)/ (Left + Right + simultaneous) (Schallert et al., 2000; Li et al., 2004; Kleim et al., 2007)

Grid-walking test. The grid-walking test was carried out as previously described (Clarkson et al., 2010, 2011), using a 12mm square wire mesh with a grid area 32cm / 20cm / 50cm (length / width / height). A mirror was placed beneath the apparatus to allow video footage of animals' stepping errors ('foot-faults'). Each mouse was placed individually atop of the elevated wire grid and allowed to freely walk for a period of 5min. Video footage was analyzed offline by raters blind as to the treatment groups. The total number of foot-faults for each limb, along with the total number of non-foot-fault steps, was counted, and a ratio between foot-faults and total-steps-taken calculated. Percent foot-faults were calculated by: [#foot-faults / (#foot-faults + #non-foot-fault steps) * 100]. A ratio between foot-faults and total-steps-taken was used to take into account differences in the degree of locomotion between animals and trials. A step was considered a foot-fault if it was not providing support and the foot went through the grid hole. Further, if an animal was resting with the grid at the level of the wrist, this was also considered a fault. If the grid was anywhere forward of the wrist area then this was considered as a normal step.

Protein extraction and Western blot analysis

Mice were sacrificed by overdose of halothane and rapidly decapitated. Brains were placed in a mouse matrix in which a 2 mm coronal section was cut , -1 mm to +1 mm from bregma. This section included the whole ischemic area (left hemisphere) and cognate regions from the contralateral uninjured hemisphere (**Figure 1B**). The tissue section was cut sagittally along the midline and both hemispheres were separately frozen in dry ice

for biochemical analysis. Protein extracts were prepared by homogenizing whole brain hemisphere samples in T-per (Pierce) extraction buffer (150 mg/ml), complemented with a protease (Complete Mini Protease Inhibitor Tablets, Roche) and phosphatase inhibitors (5 mmol/L sodium fluoride and 1 mmol/L sodium orthovanadate, Sigma), followed by centrifugation at 100,000 x *g* for 1 hour. Protein concentration in the supernatant was determined using the Bradford assay (Bio-Rad). We analyzed the expression of both forms of BDNF (precursor and mature), their receptor (TrkB) and GNDF. Equal amounts of protein per sample (10-20 µg, depending on protein of interest), were loaded in 4 to 12% gradient Bis-Tris gels (Invitrogen, Carlsbad, CA) and transferred to nitrocellulose membranes using the iblot system from Invitrogen. Membranes were blocked for 1 hour in 5% (v/v) suspension of nonfat milk or bovine serum albumin in 0.2% Tween 20 Tris-buffered saline (pH 7.5), and processed as described (Martinez-Coria et al., 2010). The primary antibodies used for Western blots were anti-VEGF (1:1000, Millipore), anti-GDNF, (1:1000, Abcam), anti-BDNF (1:1000, Abcam), anti-Trk-B (1:1000, Abcam), anti-phospho-Trk-B (1:500, Abcam). Quantitative densiometric analyses were performed using the Gel Analyzer Plugin for ImageJ 1.40g.

Histology

Mice were sacrificed by overdose of halothane, and perfused transcardially with 0.9 % NaCl followed by 4% paraformaldehyde in phosphate-buffered saline, pH 7.4, 28 days after photothrombosis. The brains were removed from the skull, post-fixed for a further 2 hours and then transferred to buffered 30% sucrose overnight or until the brains had sunk to cryoprotect. Forty-µm frozen sections were cut with a cryostat microtome (Leica, Nussloch, Germany) and stored in a cryoprotectant solution pending further processing.

Nissl stain and infarct measurement. Every third section was collected to quantify infarct volumes using cresyl violet (Nissl) stain (Ohab et al., 2006; Clarkson et al., 2010). Using StereoInvestigator software, the area of infarction on each section was quantified by measuring the ipsilateral hemisphere (excluding the infarct) relative to the contralateral hemisphere. The volume was quantified relative to section thickness and distance between sections. Sections derived from intact, operated, and sham-operated animals were analyzed. Because

no differences were detected between the patterns of staining in the cerebral cortex of intact animals and those found in cortex contralateral to the infarcted hemisphere in operated animals, in each subject the contralateral hemicortex served as control.

Immunohistochemistry. Immunohistochemical staining of glial fibrillary acidic protein (GFAP), neuronal nuclear antigen (NeuN) and platelet endothelial cell adhesion molecule (PECAM-1) were used to evaluate gliosis, neuronal and blood vessel density, respectively. Brightfield immunohistochemistry was performed using biotinylated secondary antibodies (Vector, Burlingame, CA), biotin-avidin-peroxidase complex (Vector) and diaminobenzidine (DAB, Vector) as the developing agent as described (Myer et al., 2006). Primary antibodies were: rabbit anti-GFAP (1:10,000; Dako), rat ant-PECAM-1 (1:400; BD pharmigen), bio-NeuN (1:2500; Millipore).

Image analysis. Stained sections were examined and photographed using brightfield microscopy (5X magnification) with the same microscope settings (Zeiss, Oberkochen, Germany) and on the same day. Image analysis was conducted using ImageJ 1.40g (Rasband 1997). Prior to any quantification, contrast in all the original images was automatically and uniformly adjusted using the ImageJ Enhance Contrast plugin (0.4% saturated pixels). The contralateral hemicortex served as a control. Immunohistochemical images from animals with stroke were analyzed from the end of the scar to a lateral distance of 2100 μm, divided into 6 regions (350 μm width, height was thickness of cortex; **Figures 2, 5, 6**). Sham treated animals were analyzed over identical cortical regions. Because post-stroke scarring causes changes in cortical thickness, all measures were normalized to the area of the region analyzed. For GFAP quantification, the original color images were decomposed into their color channels (blue, green and red) and the green image was chosen for posterior analysis as it exhibited the greatest contrast. An arbitrary threshold of intensity of 100 was established for all images and the percent area occupied by GFAP inmunoreactivity in each area was measured automatically. For NeuN quantification the color images were binarized and a threshold area of $7\mu m^2$ was established. The percent area occupied by NeuN immunoreactivity in each region was measured using the ImageJ Analyze Particles Plugin. For determination of cell size, individual cells were selected in Area 1 (closest to the scar; **Figure 2**),

and areas were determined using ImageJ Cell Counter and Analyze Particles Plugins and then averaged. For PECAM-1 quantification the background for each color was subtracted and the resulted images were binarized. For vascular quantification, in order to evaluate tubelike structures, a minimal threshold of $10\mu m^2$ and maximum circularly of 0.5 was established with ImageJ Analyze Particles Plugin. The percentage of each region occupied by PECAM-1 immunoreactivity and the size of individual pixel clusters were measured and then averaged. For glial scar quantification, the scar was manually traced in GFAP images and area measured using ImageJ. For all quantifications, pixels were converted to μm (pixel size=0.738 μm)

Statistical Analysis.

Comparisons were made with Student's t test, one way ANOVA, and repeated-measures one way ANOVA using Prism 4.0 (Graph Pad Software, San Diego), after verification that data were appropriate for parametric testing. For behavioral testing, differences between treatment groups were analyzed using two-way ANOVA with repeated measures and Newman–Keuls' multiple pair-wise comparisons for post hoc comparisons. A p value ≤ 0.05 was considered statistically significant. Data are expressed as the mean ± SEM.

Results

Identical infarct size and neuronal density in MEM- and vehicle-treated animals.

Consistent with previous work (Clarkson et al., 2010) an infarct centered 1.5mm lateral to Bregma affected primary motor cortex as well as FP and HP sensory cortex, with HP sensory cortex being more severely affected (**Figure 2A,B**). There was no difference in infarct size measured by Nissl staining between MEM- and vehicle-treated animals (**Figure 2A-C**), consistent with other work in which MEM was given more than 2 hours after ischemia (Lapchak, 2006; Babu and Ramanathan, 2009). NeuN staining was used to measure neuronal density and cell size in the peri-infarct region, and showed no difference between treated and untreated animals (**Figure 2D-H**). We concluded that MEM was not exerting neuroprotective effects using our treatment regimen.

Improved forepaw behavioral recovery in MEM-treated animals.

Despite identical infarct volumes, there was significant improvement in behavioral measures of recovery in MEM-treated mice compared to vehicle-treated animals. The cylinder test measures exploratory forelimb movements, and is commonly used to measure functional recovery from stroke (Kleim et al., 2007; Clarkson et al., 2010, 2011). Though both MEM- and vehicle-treated animals showed a significant increase in forelimb use asymmetry after stroke, MEM-treated animals showed a progressive recovery of the impaired limb, which was significant at 28 days post-stroke (**Figure 3A**). The grid-walking test is another commonly used measure of post-stroke functional recovery (Clarkson et al., 2010, 2011) which measures both fore- and hindlimb function. There was a significant increase in FP and HP foot faults after stroke and a subsequent slow recovery of function, which was more prominent in FP than HP. MEM-treated animals showed a greater reduction in foot-faults, which became significant 28 days after stroke. A non-significant improvement in HP function was also seen 28 days after stroke (**Figure 3B,C**). The combined behavioral test data indicates that MEM treatment was associated with improved functional recovery of FP, but not HP, function after stroke.

Improved functional recovery of forepaw sensory maps with MEM treatment.

We used OIS to measure FP and HP sensory maps before and after stroke. FP and HP stimulation revealed distinct regions of activation (**Figure 4A**), which were essentially abolished after stroke. FP maps showed a significant increase in area in MEM-treated compared to vehicle-treated animals at 28 days after stroke. The area of activation for both FP and HP sensory maps slowly increased during stroke recovery, but remained substantially below pre-stroke conditions for all animals, whether treated with MEM or not (**Figure 4B,C**). There was no significant difference in area of activation of HP maps with MEM treatment, and neither the increases in FP or HP maps for vehicle treated animals were significant. Our functional activation data thus showed a similar pattern to behavioral data, with improved recovery in FP but not HP function with MEM treatment.

Decreased reactive astrogliosis and increased vascular density in peri-infarct cortex of MEM-treated animals.

Stroke centered over forepaw motor cortex resulted in a consistent, full-cortical-thickness lesion, which at 28 days consisted of a core region of necrotic tissue (1.13 ± 0.12 mm^3 stroke + vehicle; 1.22 ± 0.10 mm^3 stroke + MEM). As expected in control animals, this lesion was encircled by an immediate border of mature, compact glial scar and a surrounding zone of moderate to mild reactive astrogliosis (Sofroniew, 2009) that exhibited a gradient of elevated GFAP expression that was highest near the lesion and declined until it became indistinguishable from that of the control hemisphere at distances greater than 1770 μm from the lesion border formed by the compact glial scar (**Figure 5B,C**). Vascular density, measured by PECAM1 staining of the endothelium, was maximally decreased in the immediate vicinity of the infarct lesion and exhibited a gradient of improvement, becoming indistinguishable from control hemisphere at distances greater than 2mm from the lesion border (**Figure 6B,C**). In MEM-treated animals, these gradients of changes in GFAP and PECAM1 immunoreactivity were significantly altered. Notably, the total area of GFAP expressing cells was significantly reduced in MEM-treated compared to vehicle-treated animals in each region of interest at increasing distances from the lesion border. Consequently, GFAP expression in MEM-treated animals became indistinguishable from control hemisphere beginning 750 μm from the lesion border, as opposed to 2000 μm in vehicle-treated

animals (**Figure 5D**). This difference was due to both decreased number and decreased size of GFAP-immunoreactive cells (data not shown). Furthermore, PECAM1 expression density was significantly *increased* in MEM-treated vs. vehicle treated animals within the first three zones of tissue (0-750 μm) adjacent to the lesion border (**Figure 6D,E**).

Increased BDNF pathway signaling in peri-infarct cortex of MEM-treated animals.

BDNF expression is increased during stroke recovery (Ploughman et al., 2009; Clarkson et al., 2011; Ke et al., 2011), and our findings of alterations in glial reactivity and vascular morphology motivated an examination of GDNF and VEGF. We found no difference in GDNF or VEGF expression by Western blot, in peri-infarct cortex. However, there was a significant increase in BDNF expression in MEM- compared to vehicle-treated animals in peri-infarct cortex during the period of stroke recovery. Consistent with this increase in expression, p-TrkB expression was also increased in this region (**Figure 7**).

Discussion

We have shown that chronic treatment with a clinically tolerated medication, dosed to deliver concentrations comparable to human use, results in improved stroke outcome. The improvements occurred despite the fact that it was delivered orally *after* the stroke, and the fact that neuroprotection was not observed. The translational significance of this finding is two-fold. Firstly, it suggests a treatment for stroke recovery that is clinically feasible. Secondly, it suggests that stroke recovery can be improved without the stringent time-dependency for neuroprotective treatment.

Recovery-promoting vs. neuroprotective effects of orally-dosed MEM.

MEM is an NMDA antagonist and thus would be expected to show neuroprotective effects when dosed appropriately. Indeed, MEM has been shown to be neuroprotective when given either before (Babu and Ramanathan, 2009), or within the first two hours after stroke (Chen et al., 1998; Görgülü et al., 2000; Lapchak, 2006) (however, see (Babu and Ramanathan, 2009). These studies all used intraperitoneal dosing, which would be expected to result in rapid attainment of phsysiologically relevant concentrations (1-10 μM in brain in 30min; (Chen et al., 1998)). In contrast, our delivery of MEM in drinking water would be expected to yield physiologically relevant concentrations more slowly (Minkeviciene et al., 2004), especially with reduced water consumption after recovery from anesthesia. These factors may account in part for the lack of neuroprotection seen in the present study. This lack of neuroprotection is important, as it allows us to specifically assess the effects on post-stroke recovery. MEM dosing in the present study was chosen to mimic dosing that has been shown to be effective in humans for Alzheimer's disease (Kornhuber and Quack, 1995)(Minkeviciene et al., 2004) rather than a dose that is super-physiological and likely to have undesired effects.

Improved sensorimotor recovery in MEM-treated animals.

Cylinder and grid walking tests have both been used to document stroke recovery (Clarkson et al., 2010, 2011) and OIS imaging has been used to demonstrate sensory map plasticity after stroke (Brown et al., 2007). This

study used both behavioral and physiological measures of sensorimotor cortex function to determine the effects of MEM on stroke recovery.

We observed improvements in both measures (behavior and OIS imaging) following treatment with MEM compared to vehicle. Interestingly, both showed improvement in FP, but not HP, behavior and sensory maps. This is likely due in large part to greater destruction of HP cortex by our stroke technique (**Figures 1,2**). However other explanations might also be considered. MEM is an activity-dependent blocker of NMDA receptors (Chen and Lipton, 2006; Johnson and Kotermanski, 2006). The differential use of the FP compared to HP (e.g. for exploratory activity) might account for a greater effect on FP sensory maps and behavioral function than HP. There are also intrinsic differences in FP and HP excitability and plasticity in rodents – likely in part due to their different functions – which might explain a difference in post-stroke recovery between the two cortices (David-Jürgens et al., 2008; Brown et al., 2009).

Because cylinder test and grid-walking examine both sensory and motor function, and because our infarct region affected both sensory and primary motor cortex regions, it is not possible to distinguish sensory and motor recovery mechanisms with precision. Unlike the rat where precision-reaching tasks can be employed to dissect such difference (Klein et al., 2012), the reaching task in the mouse recovers within two weeks making it difficult to tease apart sensory and motor functions (Clarkson et al., 2011). FP and HP sensory map testing is specific to sensory function, and confirms differential map plasticity in MEM-treated animals after stroke, but it is very likely that motor plasticity also occurred because of its prominent role in stroke and lesion recovery(Ramanathan et al., 2006; Jones et al., 2009). There are also extensive reciprocal connections between sensory and motor cortices, arguing that plasticity in one region would likely be accompanied by plasticity in the other. Changes in plasticity could be associated with changes in sprouting of new connections (Li et al., 2010), synaptogenesis (Clarkson et al., 2011) or unmasking of quiescent connections (Clarkson et al., 2010), among several mechanisms. Finally, sensory cortex has actually been shown to be capable of mediating motor output: whisker barrel sensory cortex in mouse mediates whisker retraction in a complementary loop with motor

cortex protraction (Matyas et al., 2010). While similar mechanisms might or might not be active in FP cortex recovery, this work raises the possibility that sensorimotor recovery might be driven by sensory recovery even in the absence of motor cortex plasticity.

Increased vascular density.

OIS maps are generated primarily by increases in blood volume or oxygenation, specific to the activated region of cortex(Grinvald et al., 1986; Frostig et al., 1990), and functional stroke recovery is correlated with increase or recovery of vascular density in peri-infarct regions (Zhang and Chopp, 2009). We found that PECAM1 staining, which outlines vascular endothelium, was increased within 0-750 μm of tissue adjacent to the lesion border in MEM-treated compared to vehicle-treated animals. This area corresponds to regions activated on OIS mapping (**Figures 1, 4**). Vascular integrity is a prerequisite for survival of peri-infarct tissue and subsequent functional recovery, and during stroke recovery, vascular and neural plasticity are linked (Ohab et al., 2006; Zhang and Chopp, 2009). It is thus likely that OIS map plasticity and behavioral recovery were mutually dependent processes in MEM-treated animals. How those changes were driven is less clear. The lack of a significant difference in VEGF between MEM- and vehicle-treated animals argues against this pathway. However BDNF signaling has been shown to be involved in angiogenesis (Kermani and Hempstead, 2007), and in developmental models, endothelial cells have been shown to secrete BDNF (Leventhal et al., 1999). BDNF polymorphisms, associated with poor stroke outcome in humans, show reduced angiogenesis in animal models (Qin et al., 2011). BDNF can also have acute effects on the OIS functional mapping response (Prakash et al., 1996).

Decreased GFAP expression.

GFAP expression is a hallmark of reactive astrogliosis (Sofroniew, 2009). Our observation of a decrease in GFAP immunoreactivity in peri-infarct cortex after MEM-treatment is consistent with other reports that improvements in stroke recovery are associated with reduced astrocytic reactivity as measured by GFAP expression (Li et al., 2005; Bacigaluppi et al., 2009). The cause of the reduced GFAP expression after MEM-

treatment in our animals is not yet clear and has several potential explanations. Reactive astrogliosis with upregulated GFAP expression can be driven by a wide variety of different molecular signals including neurotransmitters such as glutamate, small molecules such as ATP, and a large number of growth factors and cytokines (Sofroniew, 2009). A simple potential explanation for the reduction in GFAP and reactive astrogliosis could be that MEM caused a reduction of extrasynaptic glutamate signaling (Hardingham and Bading, 2010; Xia et al., 2010) reduced the production of neuronal stress-related molecules driving reactive astrogliosis in the peri-infarct cortex. MEM also blocks cortical spreading depression (Peeters et al., 2007), a phenomenon which induces astrogliosis (Sukhotinsky et al., 2011). It is possible that MEM-mediated inhibition of peri-infarct depolarizations (Lauritzen et al., 2011), which are electrophysiologically indistinguishable from spreading depression, might both reduce astrogliosis and favor improved recovery. It cannot be ruled out that MEM had a direct effect on astrocytes, but there is no evidence to support such a notion at this time. Further work is required.

Increased BDNF signaling.

BDNF has protean effects on the nervous system during development, plasticity, and repair after injury (Schinder and Poo, 2000; Nagappan and Lu, 2005). Increases in BDNF expression have been reported in peri-infarct cortex after stroke and correlate with functional recovery; conversely, attenuation of BDNF activity worsens outcome (Chen et al., 2005; Sulejczak et al., 2007). MEM treatment at levels comparable to ours has been shown to increase BDNF mRNA expression across the brain (Marvanová et al., 2001; Molinaro et al., 2009).

We observed an increase in BDNF and p-TrkB expression in MEM- compared to vehicle-treated animals after stroke. This increase was specific to the infarcted hemisphere (results were normalized to the unaffected hemisphere) and it was significantly greater in MEM- than vehicle-treated animals. The specificity of the increase to the infarcted hemisphere suggests that signaling related to peri-infarct recovery and plasticity is

relevant. The increase in MEM-treated animals suggests that MEM treatment may supplement an endogenous tendency to BDNF increase after stroke.

The mechanism of MEM-induced BDNF increase is not clear. A similar increase in BDNF and TrkB expression in rats treated with MK-801 suggests the BDNF increase might be NMDA-receptor associated (Marvanová et al., 2004; Guo et al., 2010; Al-Amin et al., 2011). However, though NMDA activity and BDNF secretion are often tightly linked in models of central nervous system plasticity; NMDA- and BDNF-mediated plasticity is typically dependent on *activation*, not suppression, of NMDA receptor activity (Baumbauer et al., 2009; Chen et al., 2010; Ninan et al., 2010). Moreover, increases in BDNF expression after stroke are reduced by treatment with MK-801, which is evidence that NMDA receptor activation, not blockade, is responsible for post-stroke BDNF increases (Dietrich et al., 2000).

To further link the association between BDNF and post-stroke recovery, we have recently reported that AMPAKINES that are able to induce BDNF levels can improve motor functions after stroke (Clarkson et al., 2011). In addition, we report that these elevations in BDNF levels are restricted to the peri-infarct regions as motor recovery could be blocked by local delivery of the decoy TrKB-Fc. Consistent with these findings, the present data would suggest a similar site of BDNF elevation and is also where we see changes in angiogenesis and modulation of astrogliosis.

Conclusions and translational relevance.

We have shown that chronic MEM treatment improves stroke outcome and sensory map recovery, in a manner that does not appear to be neuroprotective, and involves decreased reactive astrocytosis, increased vascular density, and increased BDNF expression. Because our findings affect behavior and anatomically specific functional maps, a neuronal mechanism for MEM's effects is obligatory, though it may not be the only one. MEM has been used for many years in treatment of Alzheimer's and other neurological diseases, and has

proven well tolerated in an elderly, medically complex population. More recently, MEM has been used to successfully treat post-stroke aphasia (Berthier et al., 2009), showing that it is well tolerated in a post-stroke population, as well as effective in promoting post-stroke plasticity. Further evaluation of MEM's mechanisms in post stroke plasticity, and testing of MEM in a clinical situation, appears to be warranted.

References

Al-Amin, H., Sarkis, R., Atweh, S., Jabbur, S., Saadé, N., 2011. Chronic dizocilpine or apomorphine and development of neuropathy in two animal models II: effects on brain cytokines and neurotrophins. Exp. Neurol. 228, 30–40.

Babu, C.S., Ramanathan, M., 2009. Pre-ischemic treatment with memantine reversed the neurochemical and behavioural parameters but not energy metabolites in middle cerebral artery occluded rats. Pharmacol. Biochem. Behav. 92, 424–432.

Bacigaluppi, M., Pluchino, S., Peruzzotti-Jametti, L., Jametti, L.P., Kilic, E., Kilic, U., Salani, G., Brambilla, E., West, M.J., Comi, G., Martino, G., Hermann, D.M., 2009. Delayed post-ischaemic neuroprotection following systemic neural stem cell transplantation involves multiple mechanisms. Brain 132, 2239–2251.

Baumbauer, K.M., Huie, J.R., Hughes, A.J., Grau, J.W., 2009. Timing in the absence of supraspinal input II: regularly spaced stimulation induces a lasting alteration in spinal function that depends on the NMDA receptor, BDNF release, and protein synthesis. J. Neurosci. 29, 14383–14393.

Benowitz, L.I., Carmichael, S.T., 2010. Promoting axonal rewiring to improve outcome after stroke. Neurobiol. Dis. 37, 259–266.

Berthier, M.L., Green, C., Lara, J.P., Higueras, C., Barbancho, M.A., Dávila, G., Pulvermüller, F., 2009. Memantine and constraint-induced aphasia therapy in chronic poststroke aphasia. Ann. Neurol. 65, 577–585.

Brown, C.E., Aminoltejari, K., Erb, H., Winship, I.R., Murphy, T.H., 2009. In vivo voltage-sensitive dye imaging in adult mice reveals that somatosensory maps lost to stroke are replaced over weeks by new structural and functional circuits with prolonged modes of activation within both the peri-infarct zone and distant sites. J. Neurosci 29, 1719–1734.

Brown, C.E., Li, P., Boyd, J.D., Delaney, K.R., Murphy, T.H., 2007. Extensive turnover of dendritic spines and vascular remodeling in cortical tissues recovering from stroke. J. Neurosci. 27, 4101–4109.

Carmichael, S.T., 2010. Targets for neural repair therapies after stroke. Stroke 41, S124–126.

Chen, H.-S.V., Lipton, S.A., 2006. The chemical biology of clinically tolerated NMDA receptor antagonists. J. Neurochem 97, 1611–1626.

Chen, J., Zacharek, A., Zhang, C., Jiang, H., Li, Y., Roberts, C., Lu, M., Kapke, A., Chopp, M., 2005. Endothelial nitric oxide synthase regulates brain-derived neurotrophic factor expression and neurogenesis after stroke in mice. J. Neurosci. 25, 2366–2375.

Chen, L.Y., Rex, C.S., Pham, D.T., Lynch, G., Gall, C.M., 2010. BDNF signaling during learning is regionally differentiated within hippocampus. J. Neurosci. 30, 15097–15101.

Chen, Wang, Y.F., Rayudu, P.V., Edgecomb, P., Neill, J.C., Segal, M.M., Lipton, S.A., Jensen, F.E., 1998. Neuroprotective concentrations of the N-methyl-D-aspartate open-channel blocker memantine are effective without cytoplasmic vacuolation following post-ischemic administration and do not block maze learning or long-term potentiation. Neuroscience 86, 1121–1132.

Clarkson, A.N., Huang, B.S., Macisaac, S.E., Mody, I., Carmichael, S.T., 2010. Reducing excessive GABA-mediated tonic inhibition promotes functional recovery after stroke. Nature 468, 305–309.

Clarkson, A.N., Overman, J.J., Zhong, S., Mueller, R., Lynch, G., Carmichael, S.T., 2011. AMPA receptor-induced local brain-derived neurotrophic factor signaling mediates motor recovery after stroke. J. Neurosci. 31, 3766–3775.

David-Jürgens, M., Churs, L., Berkefeld, T., Zepka, R.F., Dinse, H.R., 2008. Differential effects of aging on fore- and hindpaw maps of rat somatosensory cortex. PLoS ONE 3, e3399.

Dietrich, W.D., Truettner, J., Prado, R., Stagliano, N.E., Zhao, W., Busto, R., Ginsberg, M.D., Watson, B.D., 2000. Thromboembolic events lead to cortical spreading depression and expression of c-fos, brain-derived neurotrophic factor, glial fibrillary acidic protein, and heat shock protein 70 mRNA in rats. J. Cereb. Blood Flow Metab. 20, 103–111.

Franklin, K., Paxinos, G., 1997. The Mouse Brain in Stereotaxic Coordinates. Academic Press, San Diego.

Frostig, R.D., Lieke, E.E., Ts'o, D.Y., Grinvald, A., 1990. Cortical functional architecture and local coupling between neuronal activity and the microcirculation revealed by in vivo high-resolution optical imaging of intrinsic signals. Proc Natl Acad Sci U S A 87, 6082–6086.

Görgülü, A., Kinş, T., Cobanoglu, S., Unal, F., Izgi, N.I., Yanik, B., Küçük, M., 2000. Reduction of edema and infarction by Memantine and MK-801 after focal cerebral ischaemia and reperfusion in rat. Acta Neurochir (Wien) 142, 1287–1292.

Grinvald, A., Lieke, E., Frostig, R.D., Gilbert, C.D., Wiesel, T.N., 1986. Functional architecture of cortex revealed by optical imaging of intrinsic signals. Nature 324, 361–4.

Guo, C., Yang, Y., Su, Y., Si, T., 2010. Postnatal BDNF expression profiles in prefrontal cortex and hippocampus of a rat schizophrenia model induced by MK-801 administration. J. Biomed. Biotechnol. 2010, 783297.

Hardingham, G.E., Bading, H., 2010. Synaptic versus extrasynaptic NMDA receptor signalling: implications for neurodegenerative disorders. Nat. Rev. Neurosci. 11, 682–696.

Johnson, J.W., Kotermanski, S.E., 2006. Mechanism of action of memantine. Curr Opin Pharmacol 6, 61–67.

Jones, T.A., Allred, R.P., Adkins, D.L., Hsu, J.E., O'Bryant, A., Maldonado, M.A., 2009. Remodeling the Brain With Behavioral Experience After Stroke. Stroke 40, S136–S138.

Ke, Z., Yip, S.P., Li, L., Zheng, X.-X., Tong, K.-Y., 2011. The effects of voluntary, involuntary, and forced exercises on brain-derived neurotrophic factor and motor function recovery: a rat brain ischemia model. PLoS ONE 6, e16643.

Kermani, P., Hempstead, B., 2007. Brain-derived neurotrophic factor: a newly described mediator of angiogenesis. Trends Cardiovasc. Med. 17, 140–143.

Kinlay, S., 2011. Changes in stroke epidemiology, prevention, and treatment. Circulation 124, e494–496.

Kleim, J.A., Boychuk, J.A., Adkins, D.L., 2007. Rat models of upper extremity impairment in stroke. ILAR J 48, 374–384.

Klein, A., Sacrey, L.-A.R., Whishaw, I.Q., Dunnett, S.B., 2012. The use of rodent skilled reaching as a translational model for investigating brain damage and disease. Neurosci Biobehav Rev 36, 1030–1042.

Kornhuber, J., Quack, G., 1995. Cerebrospinal fluid and serum concentrations of the N-methyl-D-aspartate (NMDA) receptor antagonist memantine in man. Neurosci. Lett. 195, 137–139.

Lapchak, P.A., 2006. Memantine, an uncompetitive low affinity NMDA open-channel antagonist improves clinical rating scores in a multiple infarct embolic stroke model in rabbits. Brain Res. 1088, 141–147.

Lauritzen, M., Dreier, J.P., Fabricius, M., Hartings, J.A., Graf, R., Strong, A.J., 2011. Clinical relevance of cortical spreading depression in neurological disorders: migraine, malignant stroke, subarachnoid and intracranial hemorrhage, and traumatic brain injury. J. Cereb. Blood Flow Metab. 31, 17–35.

Leventhal, C., Rafii, S., Rafii, D., Shahar, A., Goldman, S.A., 1999. Endothelial trophic support of neuronal production and recruitment from the adult mammalian subependyma. Mol. Cell. Neurosci. 13, 450–464.

Li, S., Overman, J.J., Katsman, D., Kozlov, S.V., Donnelly, C.J., Twiss, J.L., Giger, R.J., Coppola, G., Geschwind, D.H., Carmichael, S.T., 2010. An age-related sprouting transcriptome provides molecular control of axonal sprouting after stroke. Nat. Neurosci 13, 1496–1504.

Li, X., Blizzard, K.K., Zeng, Z., DeVries, A.C., Hurn, P.D., McCullough, L.D., 2004. Chronic behavioral testing after focal ischemia in the mouse: functional recovery and the effects of gender. Exp. Neurol. 187, 94–104.

Li, Y., Chen, J., Zhang, C.L., Wang, L., Lu, D., Katakowski, M., Gao, Q., Shen, L.H., Zhang, J., Lu, M., Chopp, M., 2005. Gliosis and brain remodeling after treatment of stroke in rats with marrow stromal cells. Glia 49, 407–417.

Martinez-Coria, H., Green, K.N., Billings, L.M., Kitazawa, M., Albrecht, M., Rammes, G., Parsons, C.G., Gupta, S., Banerjee, P., LaFerla, F.M., 2010. Memantine improves cognition and reduces Alzheimer's-like neuropathology in transgenic mice. Am. J. Pathol. 176, 870–880.

Marvanová, M., Lakso, M., Pirhonen, J., Nawa, H., Wong, G., Castrén, E., 2001. The neuroprotective agent memantine induces brain-derived neurotrophic factor and trkB receptor expression in rat brain. Mol. Cell. Neurosci. 18, 247–258.

Marvanová, M., Lakso, M., Wong, G., 2004. Identification of genes regulated by memantine and MK-801 in adult rat brain by cDNA microarray analysis. Neuropsychopharmacology 29, 1070–1079.

Matyas, F., Sreenivasan, V., Marbach, F., Wacongne, C., Barsy, B., Mateo, C., Aronoff, R., Petersen, C.C.H., 2010. Motor control by sensory cortex. Science 330, 1240–1243.

Meisner, F., Scheller, C., Kneitz, S., Sopper, S., Neuen-Jacob, E., Riederer, P., ter Meulen, V., Koutsilieri, E., 2008. Memantine upregulates BDNF and prevents dopamine deficits in SIV-infected macaques: a novel pharmacological action of memantine. Neuropsychopharmacology 33, 2228–2236.

Minkeviciene, R., Banerjee, P., Tanila, H., 2004. Memantine improves spatial learning in a transgenic mouse model of Alzheimer's disease. J. Pharmacol. Exp. Ther 311, 677–682.

Molinaro, G., Battaglia, G., Riozzi, B., Di Menna, L., Rampello, L., Bruno, V., Nicoletti, F., 2009. Memantine treatment reduces the expression of the K(+)/Cl(-) cotransporter KCC2 in the hippocampus and cerebral cortex, and attenuates behavioural responses mediated by GABA(A) receptor activation in mice. Brain Res. 1265, 75–79.

Murphy, T.H., Corbett, D., 2009. Plasticity during stroke recovery: from synapse to behaviour. Nat. Rev. Neurosci. 10, 861–872.

Myer, D.J., Gurkoff, G.G., Lee, S.M., Hovda, D.A., Sofroniew, M.V., 2006. Essential protective roles of reactive astrocytes in traumatic brain injury. Brain 129, 2761–2772.

Nagappan, G., Lu, B., 2005. Activity-dependent modulation of the BDNF receptor TrkB: mechanisms and implications. Trends Neurosci. 28, 464–471.

Ninan, I., Bath, K.G., Dagar, K., Perez-Castro, R., Plummer, M.R., Lee, F.S., Chao, M.V., 2010. The BDNF Val66Met polymorphism impairs NMDA receptor-dependent synaptic plasticity in the hippocampus. J. Neurosci. 30, 8866–8870.

Ohab, J.J., Fleming, S., Blesch, A., Carmichael, S.T., 2006. A neurovascular niche for neurogenesis after stroke. J. Neurosci. 26, 13007–13016.

Peeters, M., Gunthorpe, M.J., Strijbos, P.J., Goldsmith, P., Upton, N., James, M.F., 2007. Effects of pan- and subtype-selective NMDA receptor antagonists on cortical spreading depression in the rat: therapeutic potential for migraine. J Pharmacol Exp Ther 321, 564–72.

Ploughman, M., Windle, V., MacLellan, C.L., White, N., Doré, J.J., Corbett, D., 2009. Brain-derived neurotrophic factor contributes to recovery of skilled reaching after focal ischemia in rats. Stroke 40, 1490–1495.

Prakash, Cohen-Cory, S., Frostig, R.D., 1996. Rapid and opposite effects of BDNF and NGF on the functional organization of the adult cortex in vivo. Nature 381, 702–706.

Qin, L., Kim, E., Ratan, R., Lee, F.S., Cho, S., 2011. Genetic variant of BDNF (Val66Met) polymorphism attenuates stroke-induced angiogenic responses by enhancing anti-angiogenic mediator CD36 expression. J. Neurosci. 31, 775–783.

Ramanathan, D., Conner, J.M., Tuszynski, M.H., 2006. A form of motor cortical plasticity that correlates with recovery of function after brain injury. Proc. Natl. Acad. Sci. U.S.A. 103, 11370–11375.

Rammes, G., Danysz, W., Parsons, C.G., 2008. Pharmacodynamics of memantine: an update. Curr Neuropharmacol 6, 55–78.

Rasband, W.S., 1997. ImageJ, US National Institutes of Health, Bethesda, Maryland, USA [WWW Document]. URL http://imagej.nih.gov/ij/

Roger, V.L., Go, A.S., Lloyd-Jones, D.M., Benjamin, E.J., Berry, J.D., Borden, W.B., Bravata, D.M., Dai, S., Ford, E.S., Fox, C.S., Fullerton, H.J., Gillespie, C., Hailpern, S.M., Heit, J.A., Howard, V.J., Kissela, B.M., Kittner, S.J., Lackland, D.T., Lichtman, J.H., Lisabeth, L.D., Makuc, D.M., Marcus, G.M., Marelli, A., Matchar, D.B., Moy, C.S., Mozaffarian, D., Mussolino, M.E., Nichol, G., Paynter, N.P., Soliman, E.Z., Sorlie, P.D., Sotoodehnia, N., Turan, T.N., Virani, S.S., Wong, N.D., Woo, D., Turner, M.B., 2012. Executive summary: heart disease and stroke statistics--2012 update: a report from the american heart association. Circulation 125, 188–197.

Schallert, T., Fleming, S.M., Leasure, J.L., Tillerson, J.L., Bland, S.T., 2000. CNS plasticity and assessment of forelimb sensorimotor outcome in unilateral rat models of stroke, cortical ablation, parkinsonism and spinal cord injury. Neuropharmacology 39, 777–787.

Schinder, A.F., Poo, M., 2000. The neurotrophin hypothesis for synaptic plasticity. Trends Neurosci. 23, 639–645.

Sofroniew, M.V., 2009. Molecular dissection of reactive astrogliosis and glial scar formation. Trends Neurosci 32, 638–647.

Sukhotinsky, I., Dilekoz, E., Wang, Y., Qin, T., Eikermann-Haerter, K., Waeber, C., Ayata, C., 2011. Chronic daily cortical spreading depressions suppress spreading depression susceptibility. Cephalalgia 31, 1601–1608.

Sulejczak, D., Ziemlińska, E., Czarkowska-Bauch, J., Nosecka, E., Strzalkowski, R., Skup, M., 2007. Focal photothrombotic lesion of the rat motor cortex increases BDNF levels in motor-sensory cortical areas not accompanied by recovery of forelimb motor skills. J. Neurotrauma 24, 1362–1377.

Thomas, S.J., Grossberg, G.T., 2009. Memantine: a review of studies into its safety and efficacy in treating Alzheimer's disease and other dementias. Clin Interv Aging 4, 367–377.

Xia, P., Chen, H.V., Zhang, D., Lipton, S.A., 2010. Memantine preferentially blocks extrasynaptic over synaptic NMDA receptor currents in hippocampal autapses. J. Neurosci. 30, 11246–11250.

Zhang, Z.G., Chopp, M., 2009. Neurorestorative therapies for stroke: underlying mechanisms and translation to the clinic. Lancet Neurol 8, 491–500.

Figure Legends

Figure 1. Experimental design and animal preparation. A. Schematic shows temporal sequence of stroke and experimental modalities. B. Image shows intact translucent mouse skull oriented for imaging. Green circle shows area exposed to photothrombosis; white and black squares show regions of interest for forepaw (FP) and hindpaw (HP) OIS map analysis. Inside the regions of interest are FP (purple) and HP (yellow) activation maps. Red lines show boundaries of tissue removed for Western blot analysis.

Figure 2. Post-stroke memantine treatment is not neuroprotective. A,B. Representative 40 μm Nissl stained sections collected 28 days after infarct for vehicle- and MEM-treated animals, respectively. C. shows mean (± SEM) infarct area (in mm3; n = 4 vehicle and 4 MEM-treated animals). There was no significant difference in infarct area. D, E, F. Representative NeuN stained sections from sham stroke-, vehicle-, and MEM-treated animals, respectively. A1-A6: regions of interest; *: infarct core. G. Percent area occupied by NeuN-positive cells in 250 μm wide regions of interest at increasing distances from infarct core (or equivalent location in sham stroke-treated animals). There was no significant difference in area between groups. H. Average area of NeuN-positive cells in region of interest closest to infarct (Area 1; n (putative cells) = 245 control, 214 Stroke + Vehicle, 248 Stroke + MEM). Both vehicle- and MEM-treated animals showed an increase in average cell size compared to sham-treated animals, but there was no significant difference between the two groups (One way ANOVA with Newman-Keuls Multiple Comparison Test; N.S.: not significant).

Figure 3. Improved behavioral recovery from stroke with MEM treatment. A. Cylinder test. Graph shows spontaneous forepaw asymmetry index, which records paw use on rearing (Index = (Left – Right)/ (Left + Right + simultaneous). The animals were recorded for 10 minutes and the impaired limb was on the right side. There was a significant improvement in forepaw asymmetry at 28 days of MEM treatment (***$p<0.001$; Repeated measures One Way ANOVA with Newman–Keuls' multiple pair-wise comparisons; 6 animals per group). B, C. Grid Walking test. Functional recovery was assessed with forelimb (B) and hindlimb (C) foot faults. There was a significant reduction in forelimb but not hindlimb foot faults at 28 days of MEM treatment ($p<0.05$, two-way ANOVA with repeated measures and Newman–Keuls' multiple pair-wise comparisons, 6 animals per group).

Figure 4. Significant recovery of forepaw sensory maps with MEM treatment. A. FP and HP sensory maps in representative vehicle (Stroke +Veh) and MEM (Stroke +Mem) treated animals , recorded 7 days before (-7), and 7, 14, 21 and 28 after photothrombosis. Last column shows overlay of pre-stroke and 28 day post-stroke maps. B, C. Area of activation (mean ± SEM, half maximal signal) for FP and HP respectively. There was a significant increase in FP, but not HP, activation area at 28 days of MEM treatment (*$p<0.05$, One-way repeated measures ANOVA with Tukey Multiple Comparison Test).

Figure 5. Decreased reactive astrocytosis in MEM-treated animals. A,B, C. Representative GFAP inmuhistochemistry from sham stroke-, vehicle- and MEM-treated groups respectively. A1-6: regions of interest; *: infarct core; arrows: glial scar. D. Percent area occupied by GFAP-positive cells, in 250 μm wide regions of interest beginning at the margin of the glial scar. There was a significant reduction in percent area occupied by GFAP-positive cells in MEM- compared to vehicle-treated animals. There was no significant difference in the area of the glial scar between MEM- and vehicle-treated animals (Inset). One-way ANOVA with Tukey Multiple Comparison Test *$p<0.05$, **$p<0.01$, ***$p<0.001$.

Figure 6. Increased vascular density in MEM-treated animals. A, B, C. Color figures show representative PECAM-1 inmuhistochemistry for sham stroke-, vehicle- and MEM-treated animals, respectively. The color insert in each figure is an amplification. Black and white figures in each panel are the same figures after image processing. D, E. PECAM-1 quantification. D. shows percent area occupied by PECAM-1 inmunoreactivity in 250 μm wide regions of interest beginning at the glial scar margin (a proxy for vascular density); E. shows the average area of each PECAM-1-positive image region (a proxy for vascular length and diameter). There was a significant difference in both measures between MEM-and vehicle-treated animals (One way ANOVA with Bonferroni post hoc testing; *$p<0.05$, **$p<0.01$, ***$p<0.001$).

Figure 7. Increased BNDF pathway signaling in MEM-treated animals. A. Quantification (mean optical density, normalized to GADPH) of Western Blots (representative blots in B.). There was a significant increase in BDNF and phospho-TrkB expression, consistent with activation of the BDNF pathway. (*$p<0.05$, Student's t test).

Figures

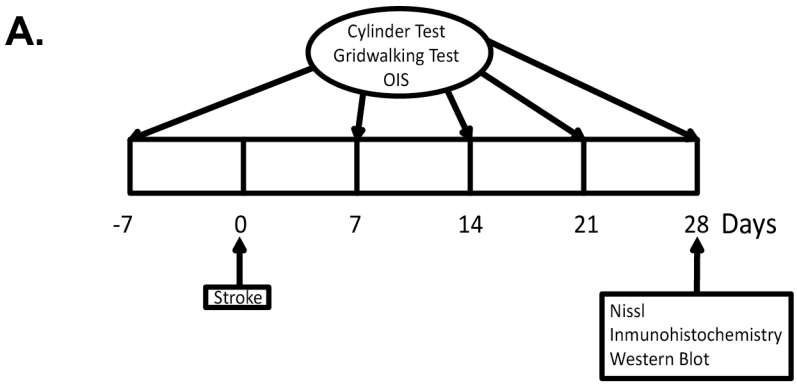

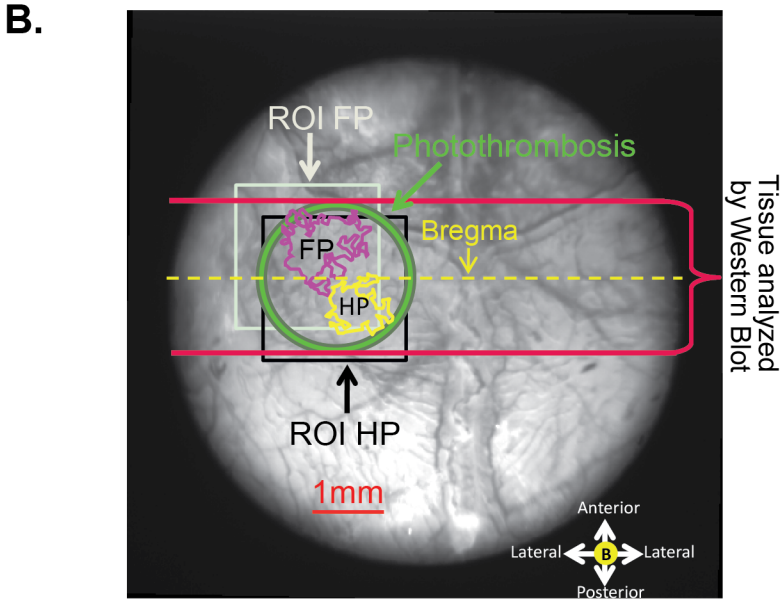

Figure 1. Experimental design and animal preparation. **A.** Schematic shows temporal sequence of stroke and experimental modalities. **B.** Image shows intact translucent mouse skull oriented for imaging. Green circle shows area exposed to photothrombosis; white and black squares show regions of interest for forepaw (FP) and hindpaw (HP) OIS map analysis. Inside the regions of interest are FP (purple) and HP (yellow) activation maps. Red lines show boundaries of tissue removed for Western blot analysis.

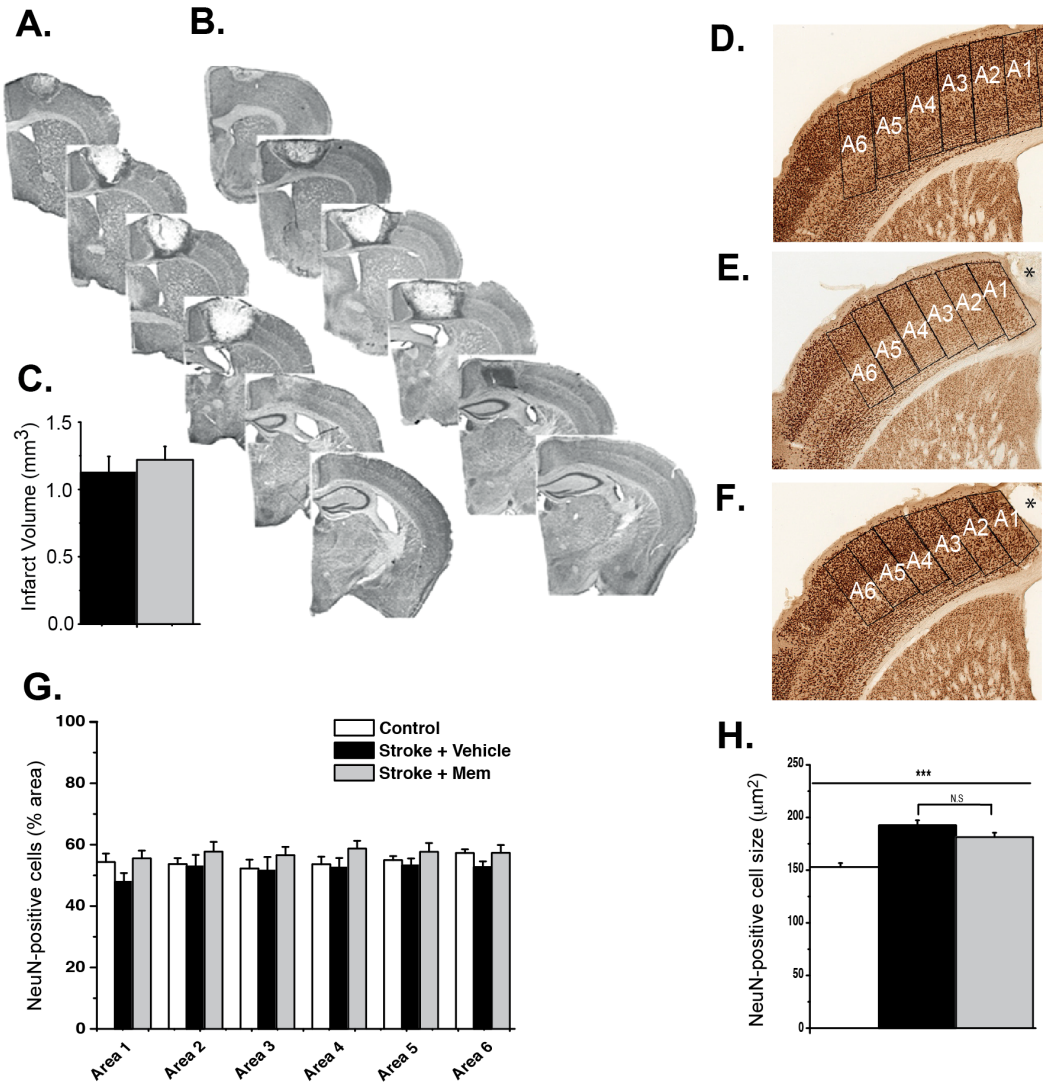

Figure 2. Post-stroke memantine treatment is not neuroprotective. A,B. Representative 40 μm Nissl stained sections collected 28 days after infarct for vehicle- and MEM-treated animals, respectively. C. shows mean (± SEM) infarct area (in mm^3; n = 4 vehicle and 4 MEM-treated animals). There was no significant difference in infarct area. D, E, F. Representative NeuN stained sections from sham stroke-, vehicle-, and MEM-treated animals, respectively. A1-A6: regions of interest; *: infarct core. G. Percent area occupied by NeuN-positive cells in 250 μm wide regions of interest at increasing distances from infarct core (or equivalent location in sham stroke-treated animals). There was no significant difference in area between groups. H. Average area of NeuN-positive cells in region of interest closest to infarct (Area 1; n (putative cells) = 245 control, 214 Stroke + Vehicle, 248 Stroke + MEM). Both vehicle- and MEM-treated animals showed an increase in average cell size compared to sham-treated animals, but there was no significant difference between the two groups (One way ANOVA with Newman-Keuls Multiple Comparison Test; N.S.: not significant).

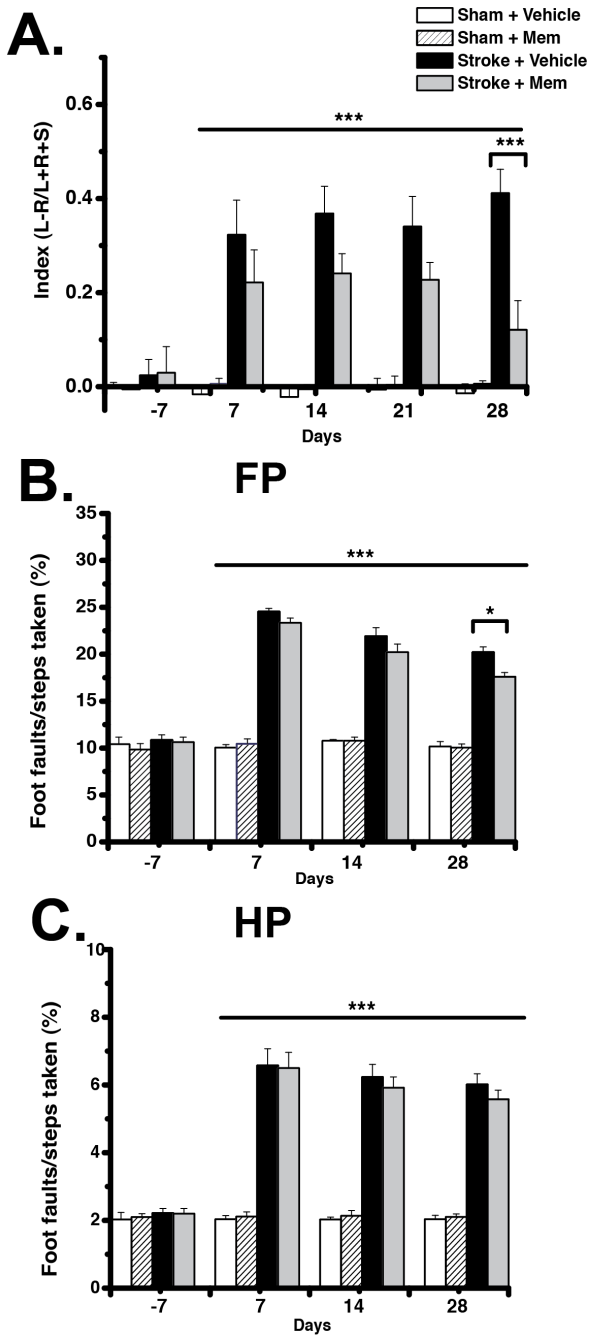

Figure 3. Improved behavioral recovery from stroke with MEM treatment. A. Cylinder test. Graph shows spontaneous forepaw asymmetry index, which records paw use on rearing (Index = (Left – Right)/ (Left + Right + simultaneous). The animals were recorded for 10 minutes and the impaired limb was on the right side. There was a significant improvement in forepaw asymmetry at 28 days of MEM treatment (***$p<0.001$; Repeated measures One Way ANOVA with Newman–Keuls' multiple pair-wise comparisons; 6 animals per group). B, C. Grid Walking test. Functional recovery was assessed with forelimb (B) and hindlimb (C) foot faults. There was a significant reduction in forelimb but not hindlimb foot faults at 28 days of MEM treatment ($p<0.05$, two-way ANOVA with repeated measures and Newman–Keuls' multiple pair-wise comparisons, 6 animals per group).

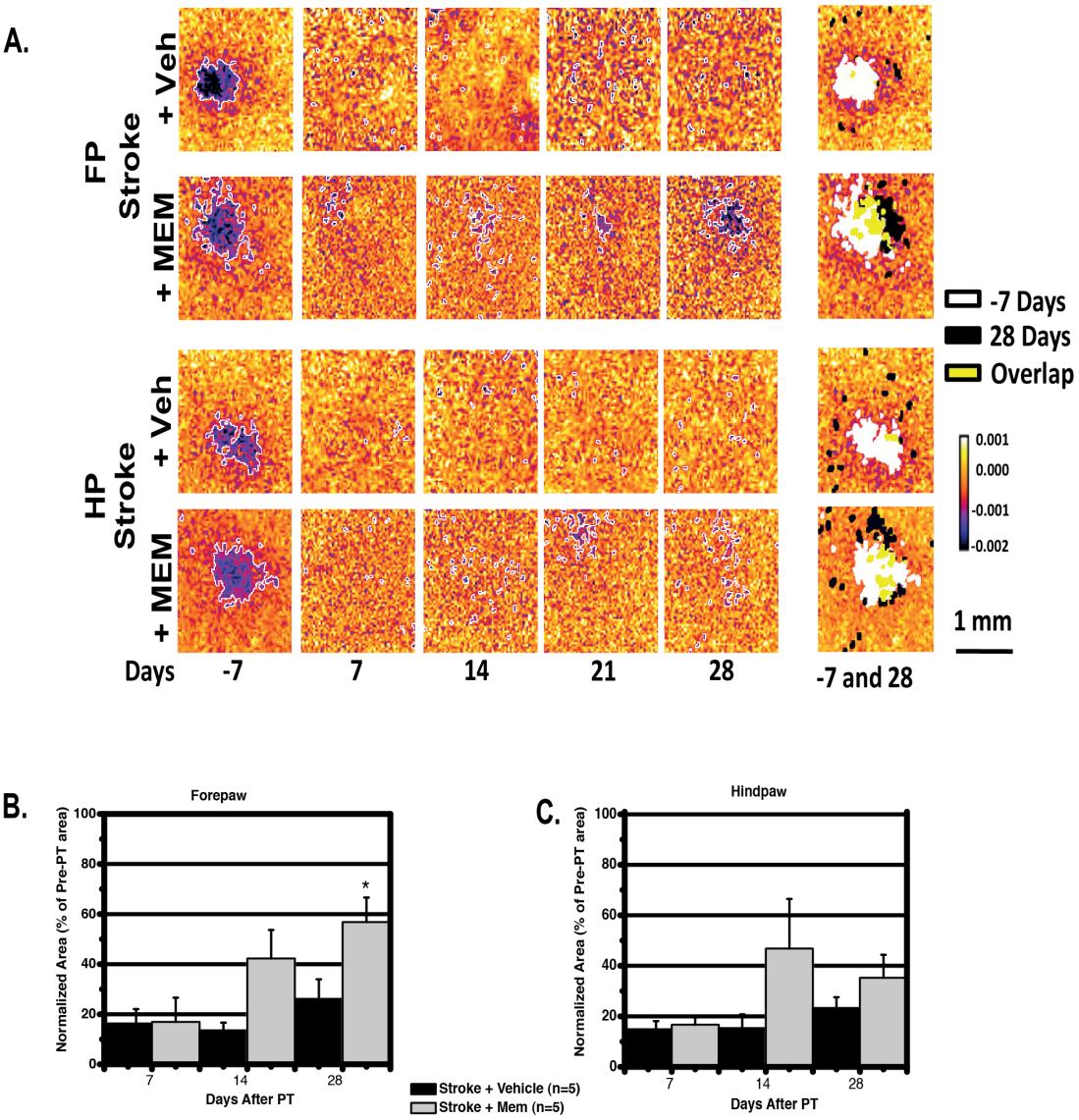

Figure 4. Significant recovery of forepaw sensory maps with MEM treatment. A. FP and HP sensory maps in representative vehicle (Stroke +Veh) and MEM (Stroke +Mem) treated animals , recorded 7 days before (-7), and 7, 14, 21 and 28 after photothrombosis. Last column shows overlay of pre-stroke and 28 day post-stroke maps. B, C. Area of activation (mean ± SEM, half maximal signal) for FP and HP respectively. There was a significant increase in FP, but not HP, activation area at 28 days of MEM treatment (*p<0.05, One-way repeated measures ANOVA with Tukey Multiple Comparison Test).

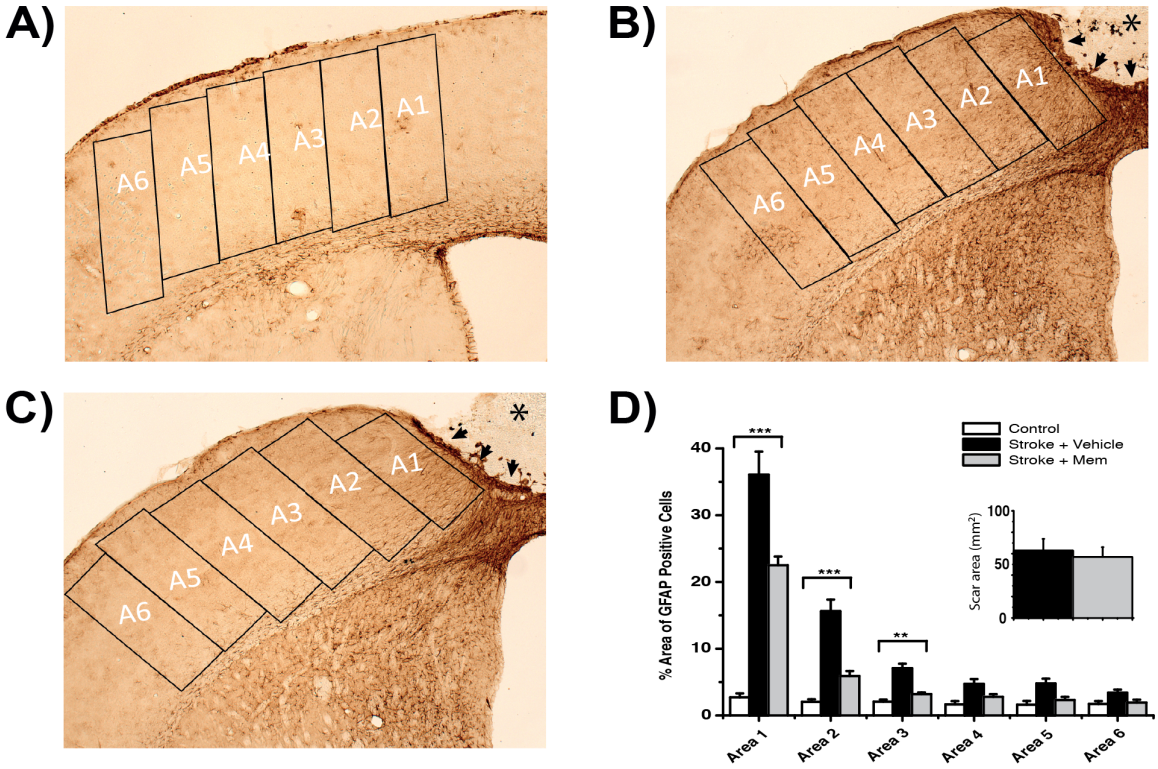

Figure 5. Decreased reactive astrocytosis in MEM-treated animals. A,B, C. Representative GFAP inmuhistochemistry from sham stroke-, vehicle- and MEM-treated groups respectively. A1-6: regions of interest; *: infarct core; arrows: glial scar. D. Percent area occupied by GFAP-positive cells, in 250 µm wide regions of interest beginning at the margin of the glial scar. There was a significant reduction in percent area occupied by GFAP-positive cells in MEM- compared to vehicle-treated animals. There was no significant difference in the area of the glial scar between MEM- and vehicle-treated animals (Inset). One-way ANOVA with Tukey Multiple Comparison Test *p<0.05, **p<0.01, ***p<0.001.

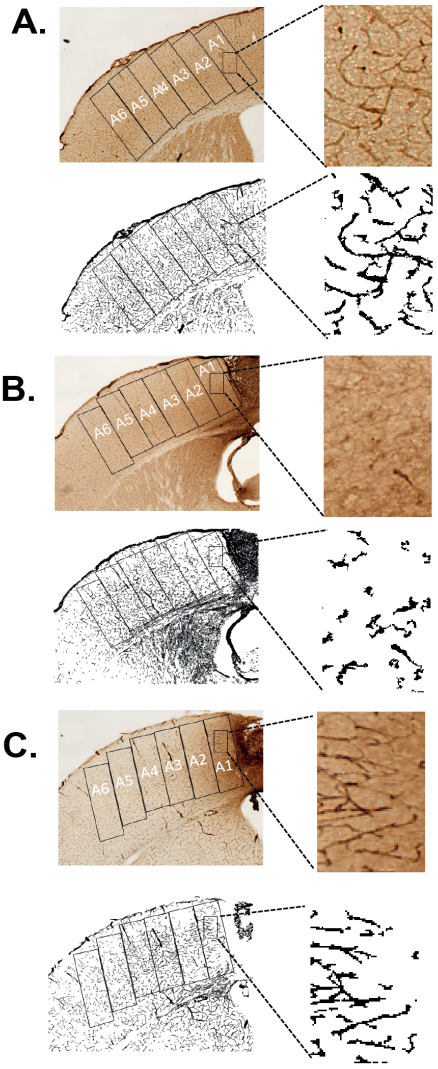

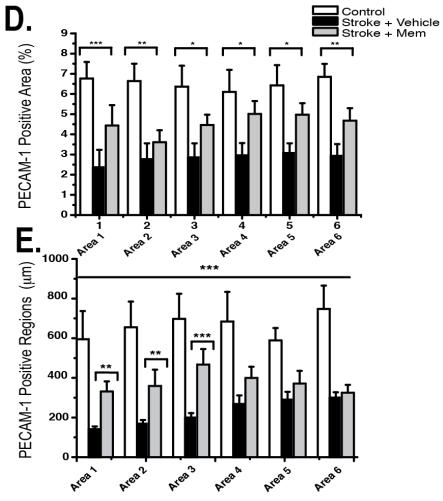

Figure 6. Increased vascular density in MEM-treated animals. A, B, C. Color figures show representative PECAM-1 inmuhistochemistry for sham stroke-, vehicle- and MEM-treated animals, respectively. The color insert in each figure is an amplification. Black and white figures in each panel are the same figures after image processing. D, E. PECAM-1 quantification. D. shows percent area occupied by PECAM-1 inmunoreactivity in 250 µm wide regions of interest beginning at the glial scar margin (a proxy for vascular density); E. shows the average area of each PECAM-1-positive image region (a proxy for vascular length and diameter). There was a significant difference in both measures between MEM-and vehicle-treated animals (One way ANOVA with Bonferroni post hoc testing; *p<0.05, **p<0.01, ***p<0.001).

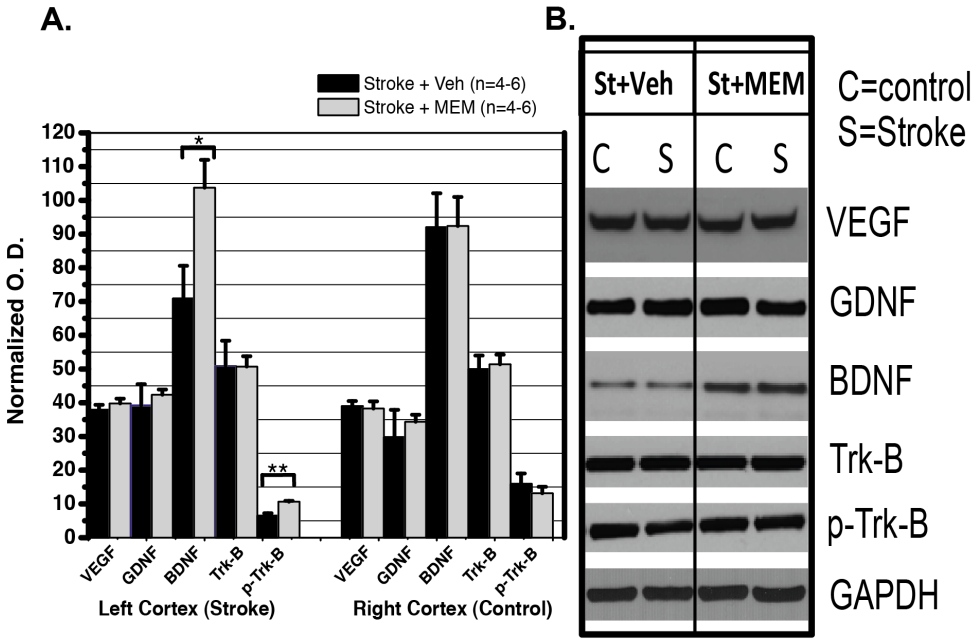

Figure 7. Increased BNDF pathway signaling in MEM-treated animals. A. Quantification (mean optical density, normalized to GADPH) of Western Blots (representative blots in B.). There was a significant increase in BDNF and phospho-TrkB expression, consistent with activation of the BDNF pathway. (*$p<0.05$, Student's t test).